CONTROLLED BALLISTIC TRAJECTORY FOR SMALL CALIBER SPIN-STABILIZED SMART MUNITIONS

A Thesis

Presented to the Faculty of the Graduate School

of Cornell University

In Partial Fulfillment of the Requirements for the Degree of

Master of Science

by

Boris Kogan

May 2014

ABSTRACT

The dynamics of bullets is examined to develop an approach for their active controls. The precession and nutation is observed to be the dominant modes in their trajectory and sufficiently slow to be perturbed. Different flow effectors are considered and *a novel low bandwidth actuation scheme is introduced*. The control approach with this new actuation scheme requires bandwidths no higher than the spin rate of the projectile. An optimal control is developed to maximize the trajectory correction within the control authority. It is shown that *a more tractable controller*, i.e., less computationally intensive, *can be developed by utilizing the natural dynamics of precession and nutation in spinning rigid bodies*.

BIOGRAPHICAL SKETCH

Boris Kogan received his B.S. in Mechanical Engineering from the Technion in 2005. Following graduation he worked for 6 years in R&D at the Israeli Ministry of Defense. Boris started his graduate studies towards a PhD degree at 2011.

ACKNOWLEDGMENTS

This work was performed as an independent study in the Laboratory for Intelligent Machine Systems under Professor Ephrahim Garcia. I would like to express my gratitude to Professor Garcia for the opportunity to be part of his research group, for his valuable guidance and for providing the motivation to attempt this complicated challenge.

TABLE OF CONTENTS

LIST OF FIGURES

LIST OF SYMBOLS

x,y,z	=	position components in inertial frame, m
ϕ,θ,ψ	=	orientation components in inertial frame (roll, pitch, yaw), rad
p,q,r	=	angular velocity components in body frame, rad/s
u,v,w	=	linear velocity components in body frame, m/s
C_X	=	total axial force (drag) coefficient
ΔC_X	=	axial force (drag) coefficient increase due to control surface
C_{X0}	=	zero AoA axial force (drag) coefficient
C_{X2}	=	squared AoA axial force (drag) coefficient
C_{NA}	=	normal force (pitch) coefficient
C_{YPA}	=	Magnus force coefficient
C_{LP}	=	roll damping coefficient
C_{MA}	=	pitch force moment coefficient
C_{MQ}	=	pitch damping moment coefficient
C_{NPA}	=	Magnus force moment coefficient
$s_{()},c_{()},t_{()}$	=	sine, cosine and tangent of angle in ( )
L,M,N	=	moment components in body frame, N·m
M_a,N_a	=	actuation moments, N·m
g	=	gravitational acceleration, 9.81 m/sec^2
X,Y,Z	=	force components in body frame, N
V	=	velocity magnitude $V=\sqrt{u^2+v^2+w^2}$, m/s
W	=	projectile weight, N
ρ	=	air density, kg/m^3
D	=	projectile diameter, m
m	=	projectile mass, kg
I	=	projectile moment of inertia tensor, kg·m^2
I_x,I_y	=	projectile moment of inertia axial and transverse component, kg·m^2

$\dot{\square}$	=	time derivative of $\square$
$\tilde{\square}$	=	$\square$ in plane-fixed coordinates
x(t),x(k)	=	continuous state vector, discrete state vector
u(t),u(k)	=	continuous state space input, discrete state space input
d	=	state space constant disturbance (gravitational load, scalar)
$\hat{A},\hat{B}_u,\hat{B}_d$	=	state space matrices
$\hat{A}(k),\hat{B}_u(k),\hat{B}_d(k)$	=	discretized state space matrices
J,Q,R	=	quadratic cost function, state cost weight matrix, input cost weight matrix.
P	=	finite horizon size (hit point)
$\overline{u}(k)$	=	control inputs saturation levels at time step k (absolute value)
H,c^T	=	quadratic programming objective coefficient matrices (Hessian and Jacobian)
A,b	=	quadratic programming constraint set of equations
$\Phi(a,b)$	=	discrete state transition matrix
$S(k)$	=	initial conditions transition matrix
$T(k)$	=	disturbance transition matrix
$[I_P]$	=	identity matrix of size P.

CHAPTER 1

INTRODUCTION

Recent advances in actuation, microelectronics and aerodynamic modeling have created the opportunity to actively control the flight trajectory and downrange impact point of supersonic hard launched munitions as small as rifle bullets. Just as guided missiles and steerable "smart bombs" revolutionized air strike capabilities and mission profiles, these "smart bullets" enable new precision capabilities to the warfighter on the ground. Previous work introduced several schemes to control projectiles in flight, primarily directed toward large caliber munitions. In many cases these munitions were designed for smoothbore weapons and classified as non-spinning projectiles. While this simplifies the actuation and flow control problems, it introduces inherent drawbacks to the dynamics. They are more strongly affected by disturbances and imperfections than their spin-stabilized counterparts and they must rely on actuated control surfaces to maintain stable flight. In addition, the requirement for smoothbore weapons means that these concepts cannot be implemented on munitions that are fired from standard small arms. A more desirable solution would facilitate trajectory control on spinning rifle bullets that could be used interchangeably with conventional ammunition in standard weapons as the tactical situation dictates.

Spinning projectiles induce both hard constraints and requirements to the control system, such as highly non-linear plant model, finite control horizon and high bandwidth controls and actuation requirements. The small scale spin stabilized munitions drive these requirements to the extreme, due to relatively short range, the very high spin rate that is required for gyroscopic stability and the limited packing volume for smart actuators, controllers and energy storage. Nevertheless converting .50 caliber bullets, which are used by snipers, to smart munitions is an attractive goal.

The size and range of this caliber allow for a reasonable amount of hardware onboard and a longer horizon (range) for maneuverability.

Various concepts of actuation and controlled perturbance methods have been proposed for 'smart munitions', both for spin and fin stabilized projectiles. The goal was either to minimize hit dispersion or to provide guidance capabilities for different scales of munitions. The proposed mechanisms applicable in spin stabilized projectiles can be grouped according to the trajectory perturbation method into three major categories: jet thrust mechanisms, momentum control mechanisms and aerodynamic control mechanisms. The jet thrust mechanism category encompasses mechanisms that produce jets for trajectory perturbation, such as the 'Synthetic Jets' [1] created by pulsating diaphragms and 'Active Transpiration' [2] MEMS scale valves that control flow propagation through transpiration channels, both suggested for 25 mm spinning projectiles. Mechanisms in the momentum control category gain control of a projectile's momentum by either manipulation of projectile mass distribution through internal mass motion [3], reaction to internal vibrating masses [4] or internal gyroscopes orientation control [5], suggested for 25-155 mm projectiles. The aerodynamic control mechanisms category includes various shapes and configurations of flow effectors and control surfaces such as pins [6] or flaps [7], morphing projectiles with gimbaled nose controlling projectile’s angle of attack [8, 9] and projectiles with a drag brake [10], all fitted to .30 to 155mm range of calibers. Also included in this category are the dual-spin projectiles that are split into two bodies that spin at different rates. The relative spin rate is controlled to reduce or completely cancel (de-spin) the gyroscopic spin of the section that holds the flow effectors, reducing the actuation bandwidth. Some concepts take advantage of the two bodies spinning asynchronously [11, 12], while others de-spin the flow effectors by rotating synchronously in the opposite direction of the gyroscopic spin [13, 14, 15].

The control schemes proposed in this paper are based on flaps capable of creating perturbation moments through asymmetric drag. We claim that with an appropriate actuation scheme, trajectory control shall not require bandwidths higher than the spin rate of the projectile. Furthermore, investigation of the rigid body motion and identification of the governing normal modes simplifies the dynamics model and reduces the size of a trajectory optimization problem, as well as creating optimal trajectory tracking controllers. The proposed low bandwidth actuation scheme combined with a simplified model predictive control provides performance levels that make the design and construction of a .50 steerable munitions a challenging but achievable goal.

CHAPTER 2

MODELING

Aerodynamic Model

The aerodynamic model of a spinning projectile has been known and used for almost a century now. A summary of the forces acting on spin stabilized projectile can be found in McCoy [16]. In 1990, U.S. Army Ballistic Research Lab (BRL) published the spark range measurements of aerodynamic coefficients required for accurate trajectory predictions of .50 caliber bullets [17]. The body forces acting on a spinning projectile are the gravity, the drag force, the normal force and the Magnus force.

$$\begin{pmatrix} X \\ Y \\ Z \end{pmatrix} = \underbrace{W \cdot \begin{pmatrix} -s_\theta \\ s_\phi c_\theta \\ c_\phi c_\theta \end{pmatrix}}_{\substack{Projected \\ Gravity}} - \underbrace{\underbrace{\frac{\pi}{8}\rho V^2 D^2}_{\substack{Dynamic \\ Pressure}} \cdot \begin{pmatrix} C_{X0} + C_{X2}\dfrac{\left(v^2+w^2\right)}{V^2} \\ C_{NA}\dfrac{v}{V} - \dfrac{pD}{2V}C_{YPA}\dfrac{w}{V} \\ C_{NA}\dfrac{w}{V} + \dfrac{pD}{2V}C_{YPA}\dfrac{v}{V} \end{pmatrix}}_{Aerodynamic\ Forces} - \underbrace{\begin{pmatrix} X_a \\ 0 \\ 0 \end{pmatrix}}_{\substack{Control \\ Force}} \tag{1}$$

The moments acting on the projectile are the roll damping moment, the overturning moment, the moment due to Magnus force and the transverse control moments that will be produced by the different flow effectors.

$$\begin{pmatrix} L \\ M \\ N \end{pmatrix} = \underbrace{\underbrace{\frac{\pi}{8}\rho V^2 D^2}_{\substack{Dynamic \\ Pressure}} \cdot D \cdot \begin{pmatrix} \dfrac{pD}{2V}C_{LP} \\ C_{MA}\dfrac{w}{V} + \dfrac{qD}{2V}C_{MQ} + \dfrac{pD}{2V}C_{NPA}\dfrac{v}{V} \\ -C_{MA}\dfrac{v}{V} + \dfrac{rD}{2V}C_{MQ} + \dfrac{pD}{2V}C_{NPA}\dfrac{w}{V} \end{pmatrix}}_{Aerodynamic\ Moments} + \underbrace{\begin{pmatrix} 0 \\ M_a \\ N_a \end{pmatrix}}_{\substack{Control \\ Moments}} \tag{2}$$

Once the forces are determined, the equations of motion for a spinning projectile (a 6-DOF rigid body) are formulated directly from the angular and linear momentum balance of Eqs. (3) - (4), respectively. Since the projectile is to be controlled with body-fixed actuators, the body-fixed and the plane-fixed frames are the two appropriate frames for the dynamic model formulation. The latter is a variation of the body-fixed frame with the spin component omitted. The equations of motion were presented by Cooper and Costello [18] and shown here as a reference.

$$\begin{pmatrix} \dot{u} \\ \dot{v} \\ \dot{w} \end{pmatrix} = \frac{1}{m}\begin{pmatrix} X \\ Y \\ Z \end{pmatrix} - \begin{pmatrix} p \\ q \\ r \end{pmatrix} \times \begin{pmatrix} u \\ v \\ w \end{pmatrix} = \frac{1}{m}\begin{pmatrix} X \\ Y \\ Z \end{pmatrix} - \begin{bmatrix} 0 & -r & q \\ r & 0 & -p \\ -q & p & 0 \end{bmatrix} \cdot \begin{pmatrix} u \\ v \\ w \end{pmatrix} \tag{3}$$

$$\begin{aligned} \begin{pmatrix} \dot{p} \\ \dot{q} \\ \dot{r} \end{pmatrix} &= \left[I^{-1} \right] \cdot \left\{ \begin{pmatrix} L \\ M \\ N \end{pmatrix} - \begin{pmatrix} p \\ q \\ r \end{pmatrix} \times \left[I \right] \cdot \begin{pmatrix} p \\ q \\ r \end{pmatrix} \right\} = \\ &= \begin{bmatrix} 1/I_x & 0 & 0 \\ 0 & 1/I_y & 0 \\ 0 & 0 & 1/I_y \end{bmatrix} \cdot \left\{ \begin{pmatrix} L \\ M \\ N \end{pmatrix} - \begin{bmatrix} 0 & -r & q \\ r & 0 & -p \\ -q & p & 0 \end{bmatrix} \cdot \begin{pmatrix} I_x \cdot p \\ I_y \cdot q \\ I_z \cdot r \end{pmatrix} \right\} \end{aligned} \tag{4}$$

The equations of motion presented here are given for the body-fixed frame. They could be easily augmented to support the plane-frame by expressing the forces in the plane-fixed frame and using the same linear and angular momentum balance equations. Projectile c.g. position and orientation in the inertial frame are retrieved by integrating the body frame velocities and performing Euler angles transformations, using Eqs. (5) – (6).

$$\begin{pmatrix}\dot{x}\\ \dot{y}\\ \dot{z}\end{pmatrix} = \underbrace{\begin{bmatrix} c_\theta c_\psi & s_\phi s_\theta c_\psi - c_\phi s_\psi & c_\phi s_\theta c_\psi + s_\phi s_\psi \\ c_\theta s_\psi & s_\phi s_\theta s_\psi + c_\phi c_\psi & c_\phi s_\theta s_\psi - s_\phi c_\psi \\ -s_\theta & s_\phi c_\theta & c_\phi c_\theta \end{bmatrix}}_{\text{Euler Angles Transformation}} \underbrace{\begin{pmatrix} u \\ v \\ w \end{pmatrix}}_{\substack{\text{Body} \\ \text{Frame} \\ \text{Velocities}}} =$$

$$= \underbrace{\begin{bmatrix} c_\theta c_\psi & -s_\psi & s_\theta c_\psi \\ c_\theta s_\psi & c_\psi & s_\theta s_\psi \\ -s_\theta & 0 & c_\theta \end{bmatrix}}_{\text{Euler Angles Transformation}} \underbrace{\begin{pmatrix} \tilde{u} \\ \tilde{v} \\ \tilde{w} \end{pmatrix}}_{\substack{\text{Plane} \\ \text{Frame} \\ \text{Velocities}}} \tag{5}$$

$$\begin{pmatrix}\dot{\phi}\\ \dot{\theta}\\ \dot{\psi}\end{pmatrix} = \underbrace{\begin{bmatrix} 1 & s_\phi t_\theta & c_\phi t_\theta \\ 0 & c_\phi & -s_\phi \\ 0 & s_\phi / c_\theta & c_\phi / c_\theta \end{bmatrix}}_{\substack{\text{Euler Angles} \\ \text{Transformation}}} \underbrace{\begin{pmatrix} p \\ q \\ r \end{pmatrix}}_{\substack{\text{Body} \\ \text{Frame} \\ \text{Angular} \\ \text{Velocities}}} = \underbrace{\begin{bmatrix} 1 & 0 & t_\theta \\ 0 & 1 & 0 \\ 0 & 0 & 1/c_\theta \end{bmatrix}}_{\substack{\text{Euler Angles} \\ \text{Transformation}}} \underbrace{\begin{pmatrix} \tilde{p} \\ \tilde{q} \\ \tilde{r} \end{pmatrix}}_{\substack{\text{Plane} \\ \text{Frame} \\ \text{Angular} \\ \text{Velocities}}} \tag{6}$$

The equations of motion reveal a non-linear time varying model. The model will be used to simulate projectile trajectory by numerical integration, with a total of 12 ordinary differential equations and states.

Linearized Model and Linear System Analysis

Linearization provides insight into the time variant and non-linear behavior of the spinning projectile and also provides a linear plant for linear controller synthesis. The plane-fixed frame model is the only model that can be linearized using the Jacobian (Taylor series expansion) and small angles approximation; in our case the model is linearized assuming small pitch and yaw angles, small transverse linear and angular velocity components, and neglecting products of small quantities and their change rates. The linear model we will use was derived for time derivatives, as opposed to the path derivatives linearized model presented by Cooper and Costello [18].

The forward velocity of the bullet is characterized independently by the non-linear ODE in Eq. (7), which shows that the velocity is slowed down by the drag force.

$$\dot{\tilde{u}} = -\left(\frac{\pi\rho D^3}{8m} C_{X0}\right) \cdot \frac{1}{D} \cdot \tilde{u}^2 - \frac{1}{m} X_a \tag{7}$$

The spin rate of the bullet in the linearized model is reduced by the roll damping moment alone. The spin is characterized by the linear ODE of Eq. (8), coupled with the forward velocity.

$$\dot{\tilde{p}} = \left(\frac{\pi\rho D^5 C_{LP}}{16 I_x}\right) \cdot \frac{\tilde{u}}{D} \cdot \tilde{p} \tag{8}$$

The rest of the velocities, which we call the transverse velocities, are governed by a linear ODE set and can be formulated by a linear state space equation of Eq. (9).

$$\begin{pmatrix} \dot{\tilde{v}} \\ \dot{\tilde{w}} \\ \dot{\tilde{q}} \\ \dot{\tilde{r}} \end{pmatrix} = \left[\hat{A}\right] \cdot \begin{pmatrix} \tilde{v} \\ \tilde{w} \\ \tilde{q} \\ \tilde{r} \end{pmatrix} + \left[\hat{B}_u\right] \cdot \begin{pmatrix} \tilde{M}_a \\ \tilde{N}_a \end{pmatrix} + \left[\hat{B}_d\right] \cdot g \tag{9}$$

where,

$$\left[\hat{A}\right]=\begin{bmatrix} -\left(\frac{\pi\rho D^3}{8m}C_{NA}\right)\cdot\frac{\tilde{u}}{D} & 0 & 0 & -\tilde{u} \\ 0 & -\left(\frac{\pi\rho D^3}{8m}C_{NA}\right)\cdot\frac{\tilde{u}}{D} & \tilde{u} & 0 \\ \left(\frac{\pi\rho D^4 C_{NPA}}{16I_y}\right)\cdot\tilde{p} & \left(\frac{\pi\rho D^4 C_{MA}}{8I_y}\right)\cdot\frac{\tilde{u}}{D} & \left(\frac{\pi\rho D^5 C_{MQ}}{16I_y}\right)\cdot\frac{\tilde{u}}{D} & -\left(\frac{I_x}{I_y}\right)\cdot\tilde{p} \\ -\left(\frac{\pi\rho D^4 C_{MA}}{8I_y}\right)\cdot\frac{\tilde{u}}{D} & \left(\frac{\pi\rho D^4 C_{NPA}}{16I_y}\right)\cdot\tilde{p} & \left(\frac{I_x}{I_y}\right)\cdot\tilde{p} & \left(\frac{\pi\rho D^5 C_{MQ}}{16I_y}\right)\cdot\frac{\tilde{u}}{D} \end{bmatrix}$$

$$\left[\hat{B}_u\right]=\begin{bmatrix} 0 & 0 \\ 0 & 0 \\ 1/I_y & 0 \\ 0 & 1/I_y \end{bmatrix} \quad \left[\hat{B}_d\right]=\begin{bmatrix} 0 \\ 1 \\ 0 \\ 0 \end{bmatrix}$$

The linearized model in Eqs. (7)-(9) introduces a de-coupled set of equations: forward velocity in Eq. (7) and spin rate in Eq. (8) are independent and decoupled from the transverse linear and angular velocities in Eq. (9). The velocity equation can be solved off-line and the solution can be stored in a lookup table, later to be used to predict the velocity profile through extrapolation of estimated velocity. The same method can be applied on the spin rate equation to predict spin rate. The transverse velocities model of Eq. (9) has the forward velocity component and the spin rate embedded in the 'A' matrix of the linearized model. Being able to predict the forward velocity and the spin rate allows us to treat the transverse velocities model as a Linear Time Variant (LTV) model.

The LTV model comprises two sets of complex poles which vary over the flight of the projectile, as demonstrated in Fig. 1 for a flight of 1000 m: the natural frequencies change notably while the damping ratio change is negligible. The normal modes can be identified as the gyroscopic

precession and nutation of projectile's motion: the slow frequency range ω_{slow}=16.8-40 Hz corresponds to precession. The fast frequency range corresponds to nutation ω_{fast}=193.1-206.2 Hz. Both frequency ranges are much lower than the spin rate range of the projectile (p=2.00–2.35 kHz). The normal mode's dynamics is of major interest in our search for opportunities to reduce actuation bandwidth.

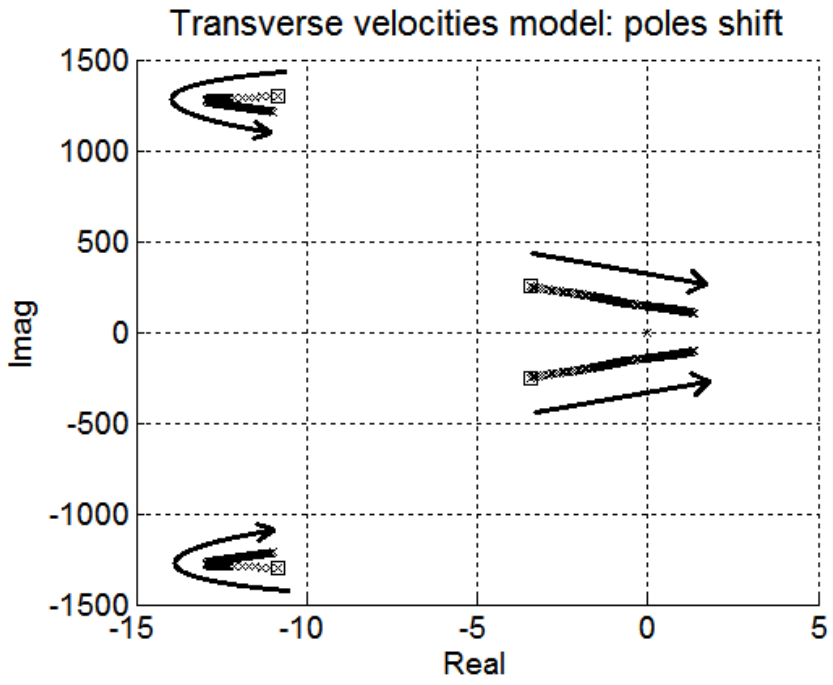

Fig. 1 Transverse velocities model: poles shift over 1000m of flight.

Finally, the expanded linearized model includes the position derivatives in the inertial frame, as shown in Eq. (10). The resulting 8th order linear model is a reduced and fully controllable LTV model to be used as the plant in trajectory control.

$$\begin{pmatrix} \dot{y} \\ \dot{z} \\ \dot{\theta} \\ \dot{\psi} \\ \dot{\tilde{v}} \\ \dot{\tilde{w}} \\ \dot{\tilde{q}} \\ \dot{\tilde{r}} \end{pmatrix} = \left[\begin{array}{cccc|cccc} 0 & 0 & 0 & \tilde{u} & 1 & 0 & 0 & 0 \\ 0 & 0 & -\tilde{u} & 0 & 0 & 1 & 0 & 0 \\ 0 & 0 & 0 & 0 & 0 & 0 & 1 & 0 \\ 0 & 0 & 0 & 0 & 0 & 0 & 0 & 1 \\ \hline & & & & & & & \\ & & 0 & & & \left[\hat{A}\right] & & \\ & & & & & & & \end{array}\right] \cdot \begin{pmatrix} y \\ z \\ \theta \\ \psi \\ \tilde{v} \\ \tilde{w} \\ \tilde{q} \\ \tilde{r} \end{pmatrix} + \left[\begin{array}{c} 0 \\ \hline \left[\hat{B}_u\right] \end{array}\right] \cdot \begin{pmatrix} \tilde{M}_a \\ \tilde{N}_a \end{pmatrix} + \left[\begin{array}{c} 0 \\ \hline \left[\hat{B}_d\right] \end{array}\right] \cdot g \qquad (10)$$

Flow Effectors

We have assumed a set of flow effectors represented as controlled moments applied on the projectile during flight. These moments, incorporated in the angular momentum balance (Eq. (2)), can be generated by aerodynamic forces. The applicable effectors in the scale of the discussed projectile caliber can be a variation of the concepts illustrated in Fig. 2. These effectors will produce perturbance moments through asymmetric drag from a controlled spoiler or a gurney flap interaction with the flow. It is believed to be possible to implement a balancing mechanism such that the deployment of the flow effector will not create a mass imbalance. The effectors are modeled as moments created by the drag asymmetry, while the additional drag itself would be small with respect to the overall drag. It will be shown later that this additional drag will marginally reduce the range of the projectile and can be taken into account in the modeling of the controlled system if needed.

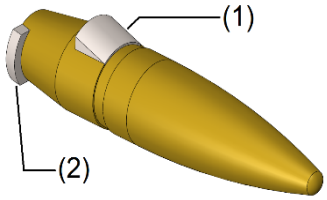

Fig. 2 Flow effector concepts: (1) – Aerodynamic spoiler, (2) – Gurney flap.

To determine the capability of the proposed effectors and their actuators, CFD results are examined for 2D axisymmetric steady state flows. The maximal amount of additional drag created by the effector will depend on the deployment height and the width of the control surface. Our initial assessment of the aerodynamic loads on the control surface is scaled to comply with actuation capacity of piezoelectric stack actuators: 2 mm maximum deployment and 8 mm control surface width. These results are mostly for providing an estimate of the control surface control authority. While the simulation might not be precise, only the resulting magnitude of the maneuverability of the controlled bullet will be affected, while the controls and actuation scheme remain valid.

The drag force acting on the projectile changes with the velocity which varies greatly during flight. Therefore, we define drag asymmetry as the ratio of drag increase, due to control surface deployment, to drag of an uncontrolled bullet ($\Delta C_X/C_X$). This ratio changes as the velocity decreases over the flight range, however for the sake of analysis simplicity and without loss of generality we will assume it to be constant, since it will only change the maneuverability and not the proposed concepts. The drag asymmetries produced by the spoiler and the gurney flap are shown in Fig. 3: the spoiler will produce the larger drag asymmetry (18%, as shown in Fig. 3a), and will create the most salient secondary shockwave (Fig. 3b).

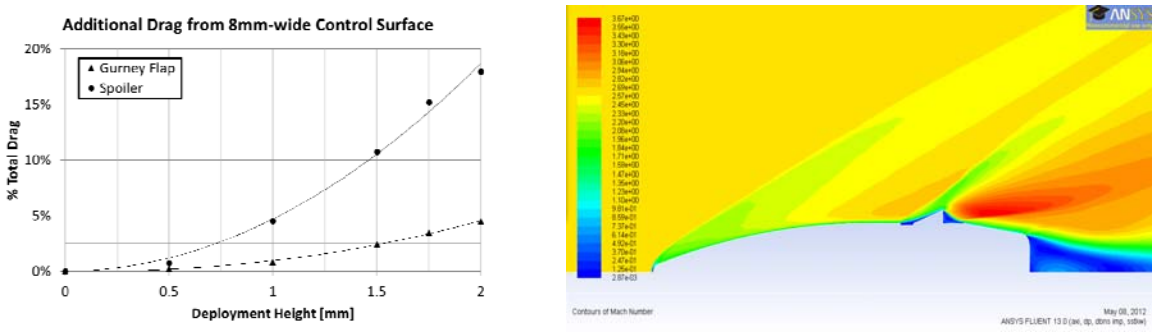

Fig. 3: (a) capacity of different control surface configurations, (b) velocity contours for the spoiler configuration.

Control saturation is present here, as in any controlled system. The saturation levels need to be either avoided or appropriately utilized to satisfy the trajectory control requirements. In our case, control saturation is the set of aerodynamic loads at maximal control surface deployment the proposed effectors can produce, as a function of velocity. The saturation levels need to be modeled to provide a prediction capability for incorporation into controller synthesis. Using the drag asymmetry definition, the control bounds can be evaluated directly from the predicted forward velocity: small pitch and yaw angles approximation omits the second order angle of attack term in the dimensionless drag coefficient (i.e. $C_X=C_{X0}$), then the aerodynamic load produced by the flow

effector is extracted directly from the definition of the drag coefficient. The saturation levels for a muzzle velocity of 890 m/s (MACH 2.7) and 15% drag asymmetry are shown in Fig. 4 as an example.

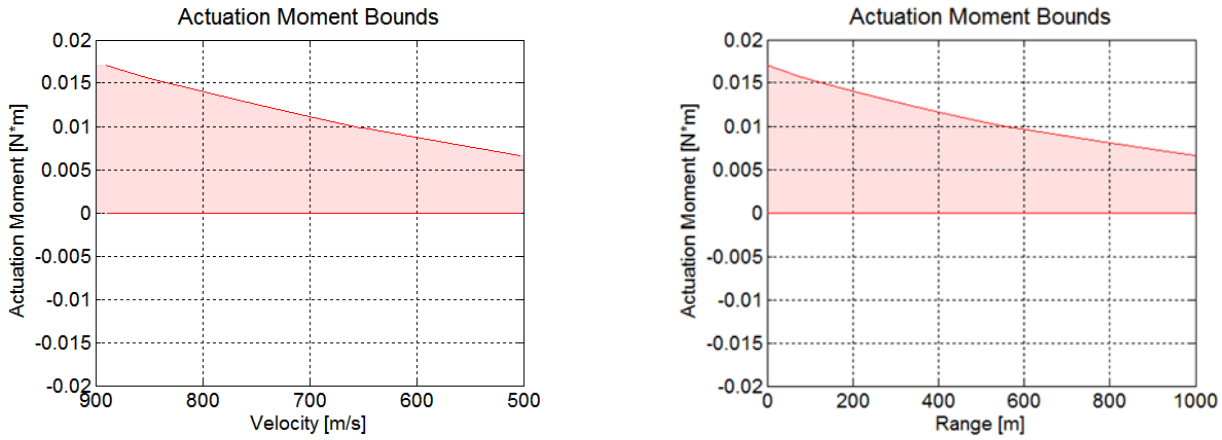

Fig. 4: Control moment saturation level: 890 m/s at muzzle, 15% drag asymmetry.

Actuation bandwidth requirements clearly represent a challenge in the control of the .50 caliber spinning projectiles. Body-fixed actuators would require a bandwidth of one to two orders of magnitude higher than the 2.35 kHz spin rate of the bullet to deploy the flow effectors for a portion of the roll cycle, with a reasonable rise time. Also, transient flow effects are bound to increase the high bandwidth requirements even further. The actuators are modeled as if capable of generating square wave displacements, keeping in mind that actuator's deployment timing can be tuned so that the flow effectors produce the same aerodynamic loads as with the square wave actuation.

CHAPTER 3

OPEN LOOP PERFORMANCE ANALYS

Uncontrolled Trajectory

First we will examine the open loop trajectory of the projectile system. The non-linear model in Eqs. (1) – (6) is integrated using 4th order Runge-Kuta numerical integration. Both the linear and angular transverse velocity components are integrated from flat-fired initial condition. Initially, the model was verified with a case study of .30 caliber bullets given in McCoy [16]. Next, we turn to study the .50 caliber trajectory. The muzzle velocity and the spin rate of a typical .50 caliber bullet (M33) are 890 m/sec (MACH 2.7) and 2.35 kHz, respectively. The maximum and optimal impact ranges of the projectile are declared to be 2000 and 1000 m, respectively. Over a 1.5 sec the projectile travels 1000 m and the velocity and the spin rate are reduced to 500 m/sec (MACH 1.5) and 2.0 kHz respectively, due to drag and roll damping moment acting on the bullet.

The uncontrolled trajectory is shown in Fig. 6, in terms of projectile's c.g. position. Two phenomena associated with the motion of a spinning rigid body are observed. The first phenomenon is a trajectory bending due to gravity, acting as a constant load and generating a downward velocity component, resulting in a 9.21 m drop over a range of 1000 m. The second phenomenon is a gyroscopic drift, associated with the gyroscopic motion of the projectile. The linear velocity vector is diverted from the angular velocity vector due to gravity, inducing an angle of attack that results in lift and an overturning moment. The overturning moment shifts the angular momentum and creates a gyroscopic drift of 0.18 m to the right (for a clockwise spin, as observed by the shooter) over a range of 1000 m as shown. In Fig. 7 we observe the precession and nutation of the gyroscopic motion through the pitch and yaw angles of the projectile. In the presence of gravity, precession and nutation integrate into a spiral motion in the inertial frame. These

phenomena change the orientation of the projectile, causing it to veer away from an intended target. To compensate, snipers range the target and adjust the targeting scope accordingly.

Single Actuator Performance

Let's consider a single deployed effector and observe the open loop dynamics of the projectile's trajectory. The basic scheme for controlling the trajectory with a single flow effector attached to a spinning body is to deploy the control surface over a prescribed sector of the roll cycle, as illustrated in Fig. 5. We will call this control scheme roll based control (RBC). As proposed earlier, the model of this flow control concept is a perturbation moment pulse acting on projectile's c.g.. The actuation bandwidth of the proposed scheme would have to be greater by at least an order of magnitude than the spin rate of the projectile. The controllable parameters in this scheme are the moment magnitude (deployment stroke, pulse height), the sector size (deployment time, width of the deployment command pulse) and the actuation phase (deployment timing, pulse orientation relative to the gravity vector).

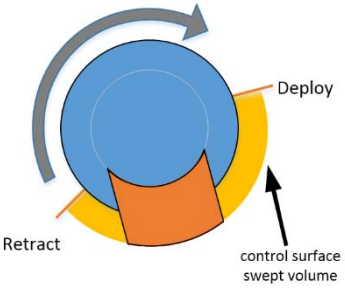

Fig 5: Roll Based Control scheme, as seen from projectile's rear view.

The RBC scheme diverts the projectile from the uncontrolled hit point and produces a noticeable change in the precession and nutation image, as illustrated in Fig. 6 and Fig. 7. The perturbing moment pulses increase the nutation angle by almost two orders of magnitude. This increased nutation angle changes the angle of attack, which results in trajectory diversion. The RBC scheme was investigated by fixing the moment magnitude to its saturation level (15% drag) and simulating different combinations of sector sizes and actuation phases, similarly to Fresconi and Plostins's work in [19]. In Fig. 9 we observe that the RBC maneuver footprint (the area covered by the controllable hit points) is circular. The dispersion radius (maneuver footprint radius) is a function of the roll sector size, symmetric about the 180° sector size. The perfectly circular maneuver footprint obtained in our study differs from the tilted ellipses presented by Fresconi and

Plostins. The reasons for this discrepancy are the initial conditions and the maneuver footprint planes: flat-fired bullets vs. shells fired from elevated barrels, vertical plane for bullets footprint vs. horizontal plane for shells. We have also observed that the hit point on the circumference of the maneuver footprint is linear to the actuation phase and decoupled from the rest of the control parameters. When we fix the roll sector and change the moment magnitude within the applicable range of 0-30% drag asymmetry, a linear relation between the dispersion radius and the moment magnitude is seen. These results imply that the model nonlinearities are not dominant in the system behavior. The maneuver footprint's linear nature invites the application of linear controllers for the trajectory.

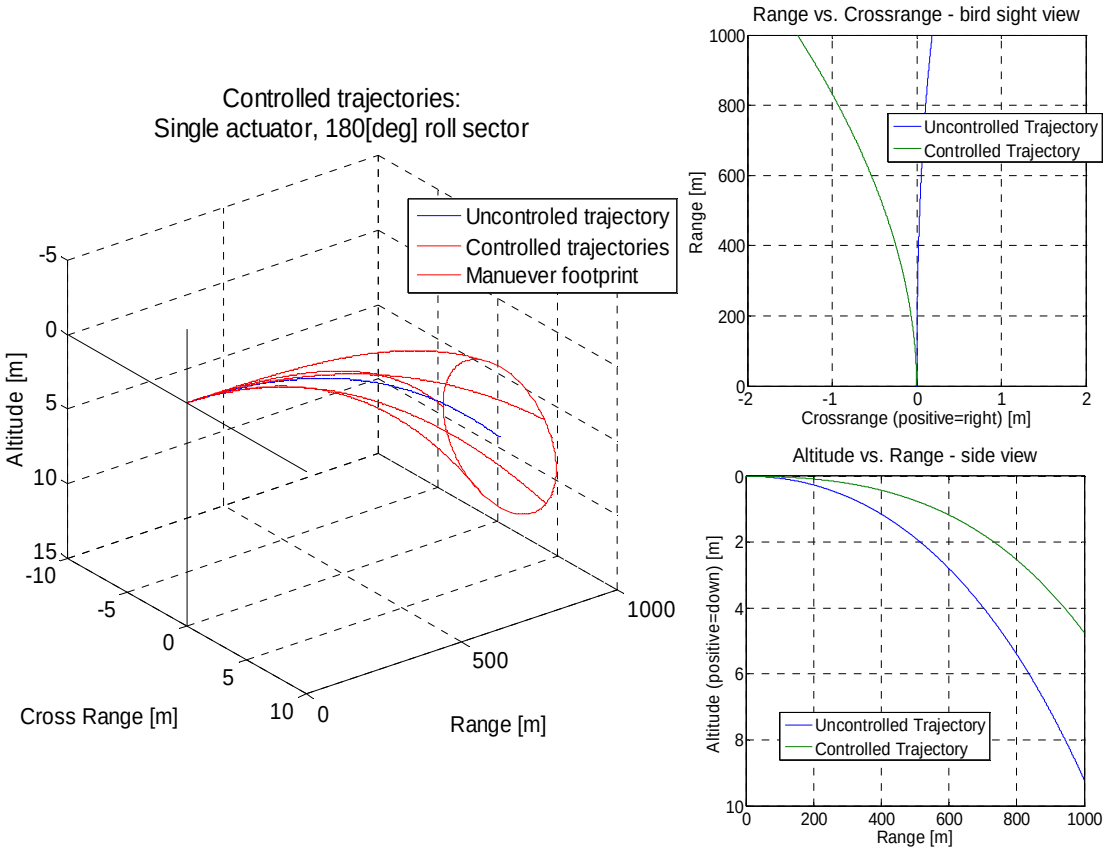

Fig. 6: Uncontrolled and single actuator Roll Controlled trajectories: c.g. position (various actuation phases, 180° sector size). Left: 3D view. Top-right: side view projection of the trajectory (72° actuation phase, 180° sector size). Bottom-right: bird sight view projection of the trajectory (72° actuation phase, 180° sector size).

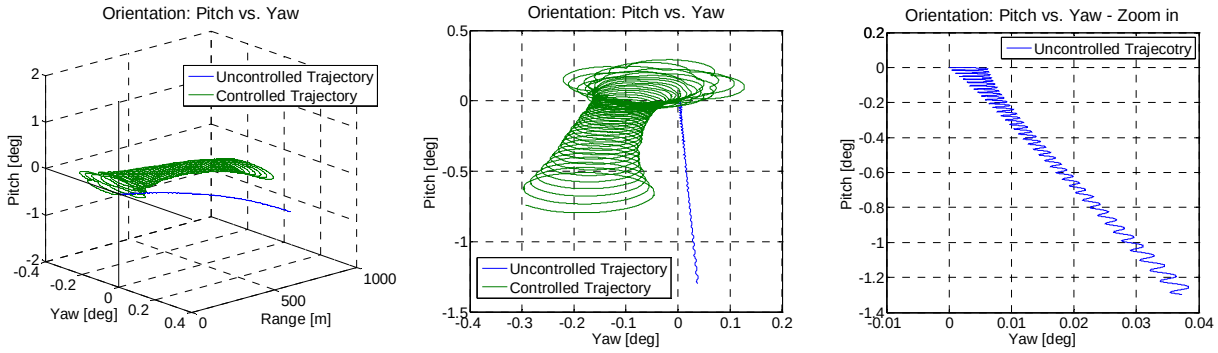

Fig. 7: Uncontrolled and single actuator Roll Controlled trajectories (72° actuation phase, 180° sector size): Projectile orientation (pitch and yaw). Left: 3D view. Middle: Planar projection. Right: Planar projection, zoom-in.

Two Bi-directional Actuators Performance for the De-spun Effect

Two bi-directional flow effectors, each capable of producing a negative actuation moment by deploying the control surface on the opposite side of the roll sector, are bound to produce a larger maneuver footprint than the single uni-directional counterpart. Moreover, the two effectors are capable of creating a moment about the projectile's c.g. in any direction, regardless of projectile's roll state. The de-spun scheme is a special configuration of two perpendicular flow effectors, oscillating sinusoidally with 90° phase between them. The scheme produces a continuous and non-rotating moment (stationary with respect to an inertial frame), as illustrated in Fig. 8. The frequency of the flow effectors must be synchronized to the spin rate of the projectile. The de-spun scheme could also be implemented with a single uni-directional flow effector, if the control surface is mounted on a de-spun section of the projectile (spinning in the opposite direction with the same rate as the overall projectile's spin) as suggested in [13] and [14]. However, de-spinning sections of the projectile of our scale is believed to be impossible due to small size and very high spin rate of a .50 caliber bullet.

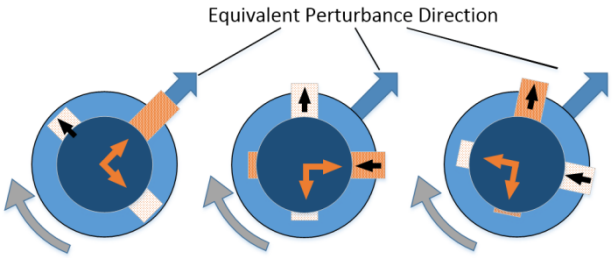

Fig. 8: De-spun flow effectors configuration.

The de-spun scheme is equivalent to a constantly deployed single actuator. It is expected to produce the largest possible maneuver footprint that can be obtained with a single flow effector. We will use this performance as a benchmark measure to evaluate how well different open and closed loop controllers perform. Fig. 9 shows that the scheme out-performs the largest RBC maneuver footprint, with a dispersion radius three times larger and the flow effector deployed only twice the time of the 180° RBC scheme. The perturbance moment exerted by the flow effector is proportional to the square of the forward velocity; hence, the deployment time is not proportional

to the dispersion radius. The de-spun scheme provides linear behaviors, as in the RBC scheme: the dispersion radius is proportional to the moment magnitude and the hit point on the circumference of the maneuver footprint is linear to the actuation phase. Here, the actuation phase is the equivalent perturbance direction of the effectors.

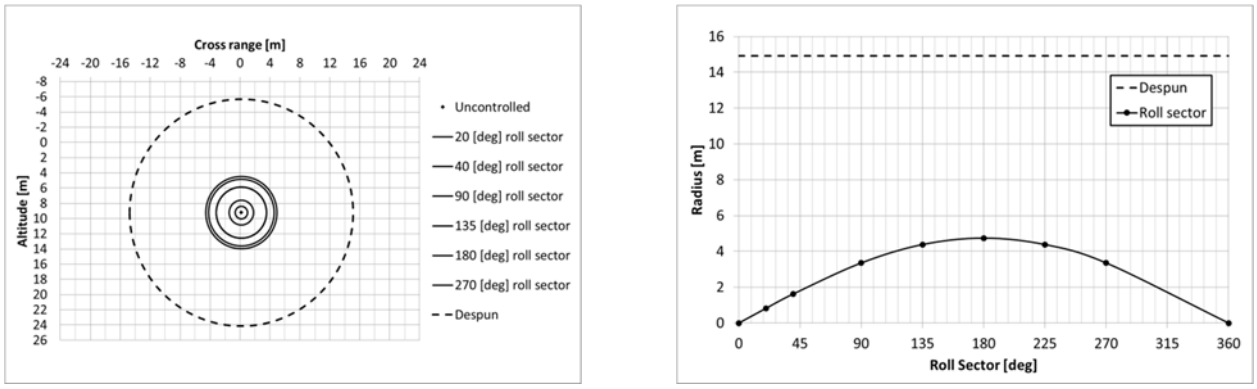

Fig. 9: Roll Based Control maneuver footprint (actuator saturation at 15% of drag, range of 1000 m). Left: footprint circles. Right: footprint radius (radius of dispersion).

Precession Synchronized Single Actuator Performance

A close look into the precession and nutation of the RBC trajectory (Fig. 7) reveals that the scheme has various impacts on nutation when the perturbation moments are applied at different precession and nutation states. The projectile is governed by a gyroscopic motion, thus the perturbations shift the momentum between angular velocity components, resulting in nutation angle increase. Flow effector deployment at certain instances increases or decreases the nutation angle, depending on the state of the precession. This observation implies that the magnitude of the nutation angle can be controlled in open loop by synchronizing the RBC scheme with the precession rate and thus creating a new scheme of Precession Synchronized Roll Based Control (PSRBC). Fig. 10 illustrates the PSRBC scheme, where the precession angle is the transverse component of the angular velocity. In order to increase the nutation angle, the flow effector deployment will be inhibited (by masking the actuation command) at the precession states where the nutation would be reduced, and vise-versa.

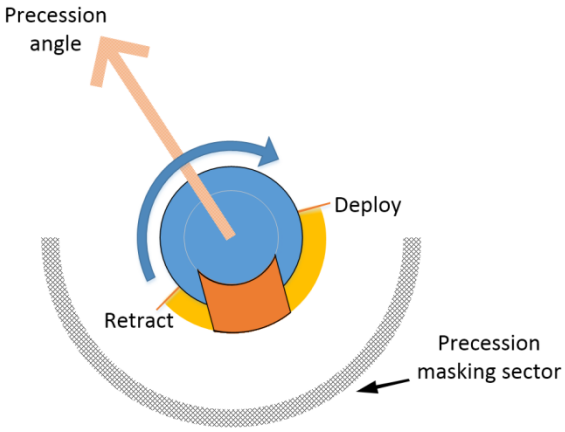

Fig 10: Precession Synchronized Roll Based Control scheme, as seen from projectile's rear view.

The PSRBC scheme nutation control is demonstrated in Fig. 11: certain combinations of roll and precession masking sectors (in-phase masking) are able to increase the nutation angle to approximately 1° over 1000 m range (Fig. 11.a), while others (out-of-phase masking) minimize the nutation to levels as low as unperturbed (uncontrolled) trajectories.

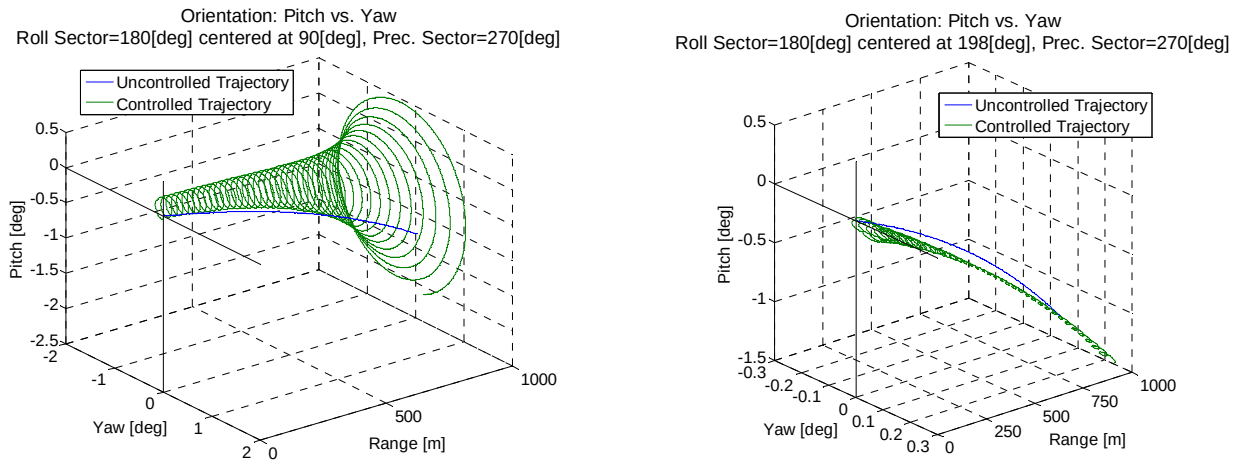

Fig. 11: Uncontrolled and single actuator Precession Synchronized trajectories: Projectile orientation (pitch and yaw). Fig. 11.a (left): In-phase masking: increasing nutation angle. Fig 11.b (right): Out-of-phase masking: decreasing nutation angle.

While increasing the nutation angle by two orders of magnitude, the PSRBC scheme does not exceed the bounds of the RBC scheme, as demonstrated in Fig. 12. The footprints were generated with different roll sector sizes, roll actuation phases and different precession masking sectors. Applying PSRBC to the maximal RBC footprint (180° roll sector) reduced the footprint to a smaller and non-circular shape. However when applying PSRBC to a smaller RBC footprint (a 270° roll sector, for example), we get a footprint that covers an area beyond the original footprint. The PSRBC footprints can be rotated around the uncontrolled hit point by adjusting the precession masking sector phase (precession masking sector orientation relative to the gravity vector), and thus swept into circular footprints. The projectile does not lose any maneuverability with the PSRBC scheme, but gains the ability to control the transverse angular velocity components. This creates an incentive to produce a closed loop controller that expands and contracts the nutation angle as a medium to create larger trajectory diversions. Active expansion and contraction of the nutation can produce a spiral diversion of the angular velocity vector, as in 'walking the precession', and will be shown next.

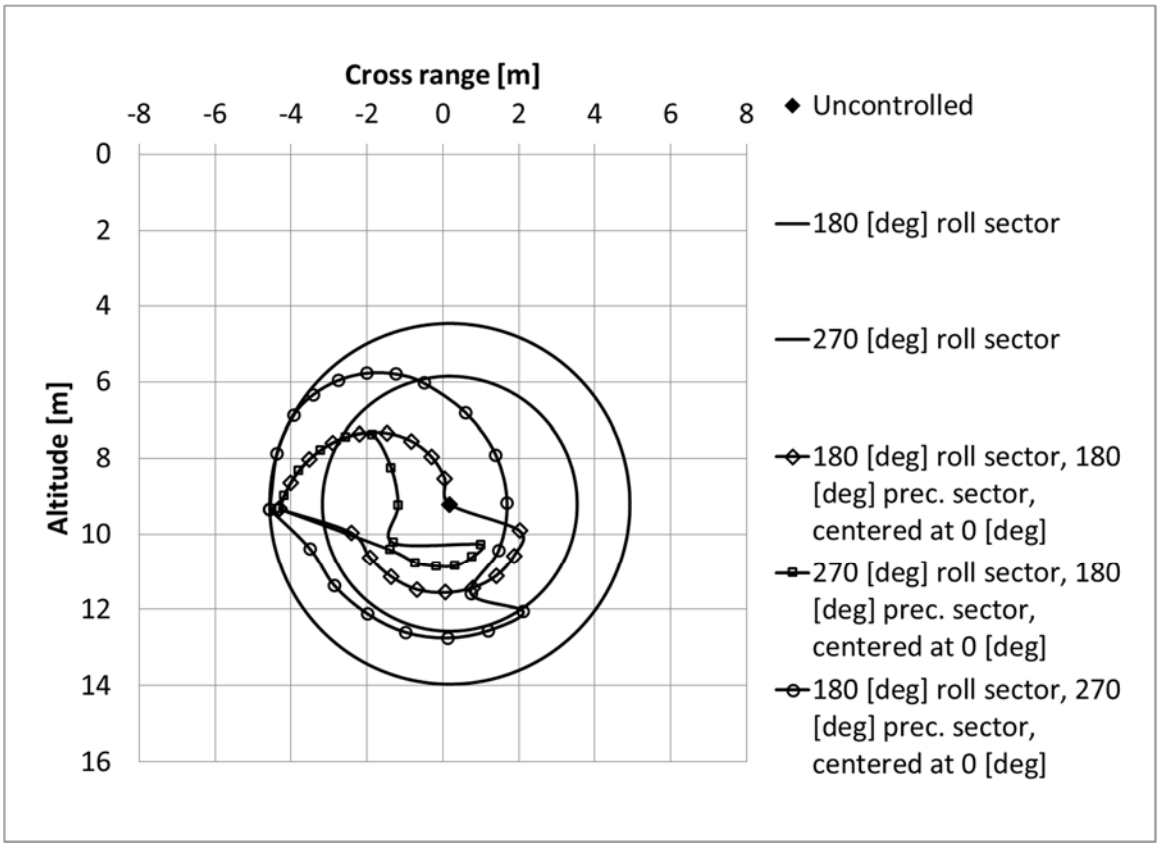

Fig. 12: Precession Based Control maneuver footprint (actuator saturation at 15% of drag, range of 1000 m).

The impact of additional axial drag

The assumption of the marginal impact of additional drag was tested for the different open loop control schemes. Fig. 13 shows the kinetic energy of the projectile during flight. Our point of interest is the impact point. We observe that the de-spun scheme impacts the trajectory the most, as expected, with approximately 5% decrease in kinetic energy. This affects the time of flight of the bullet but does not affect the range.

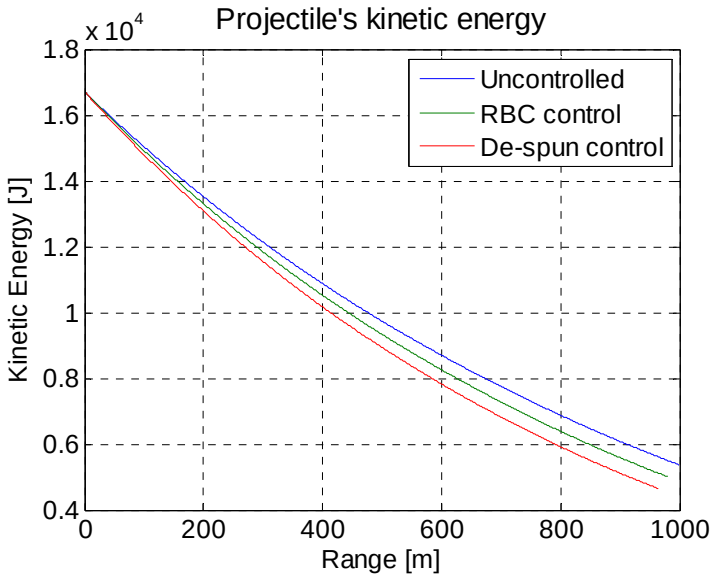

Fig. 13: Projectile's kinetic energy in different actuation schemes.

CHAPTER 4

TRAJECTORY CONTROL

Actuation Schemes and Control Approaches

Using the insights from the open loop performance analysis, we turn to search for appropriate close loop controllers. Several aspects need to be addressed in the controller design. As the control surface actuators are limited to a finite stroke, the control moments have saturation limits. Designing a controller that never saturates the control moment would limit performance. Moreover, in multiple flow effectors schemes an effort needs to be made to maintain the control vector direction when one of the actuators saturates, further limiting performance. In addition, receding horizon needs to be addressed. To maximize the control authority, the trajectory has to be regulated within a fixed range, where the projectile reaches the target exactly at the hit point and not before. Finally, in order to maximize maneuverability, all of the control authority should be transformed into projectile's momentum and the excess control authority stored in the angular momentum in the form of increased nutation angle. The stored control authority can be later used to regulate reference signal changes and reject disturbances if required.

We will use the de-spun control scheme to maximize the control authority, while minimizing the actuation bandwidth requirement to be in the spin rate's order of magnitude. The de-spun scheme is spin invariant, so we can use the linearized model as the plant model. To address the challenges of control saturation, finite horizon and control allocation, we will generate an optimal trajectory that minimizes a quadratic cost function and satisfies the saturation and the finite horizon constraints. Different tracking controllers will be used to track the optimal trajectory and reject disturbances.

Optimal Projectile Trajectory

To generate a finite horizon optimal trajectory we discretize the linear plant model and setup a finite discrete quadratic cost function in Eq. (11).

$$J = \frac{1}{2}\sum_{n=0}^{P} x(n)^T \cdot Q \cdot x(n) + u(n)^T \cdot R \cdot u(n) \tag{11}$$

The optimal trajectory that obeys control saturation limits will be found using quadratic programming. The cost function and the control input constraints need to be transformed into the quadratic programming form in Eq. (12). The quadratic cost function is the quadratic programming objective that shall be minimized, and the control saturation levels are the constraints.

$$\begin{aligned} &\min : J = \frac{1}{2} u^T \cdot H \cdot u + c^T \cdot u \\ &subject\,to: \\ &\qquad A \cdot u \le b \end{aligned} \tag{12}$$

where,

$$u = \begin{bmatrix} u(0) & u(1) & \cdots & u(p-1) \end{bmatrix}^T$$

The quadratic programming problem will be solved for a set of discrete open loop inputs that generate the optimal trajectory. To produce the Hessian (H), the Jacobian (cT) and the constraint equations set (A, b) of the quadratic programming problem, the state space solution in Eq. (13) is plugged into the quadratic cost of Eq. (11).

$$\begin{aligned} x(n) = \Phi(0, n-1) \cdot x(0) + \sum_{m=0}^{n-1} \Phi(m+1, n-1) \cdot B_u(m) \cdot u(m) + \\ + \sum_{m=0}^{n-1} \Phi(m+1, n-1) \cdot B_d(m) \cdot d \end{aligned} \tag{13}$$

where,

$$\Phi(a,b) \equiv \prod_{l=a}^{b} A(a+b-l)$$

The linear and quadratic terms are collected and the constant terms are omitted, resulting in the abbreviated quadratic cost function of Eq. (14).

$$\begin{aligned} J = & \sum_{n=1}^{P}\sum_{m=0}^{n-1}\left[\left[S(n)^T + T(n)^T\right]\cdot\left[\Phi(m+1,n-1)\right]\cdot B_u(m)\right]\cdot u(m) + \ldots \\ & + \frac{1}{2}\sum_{n=1}^{P}\left[\sum_{q=0}^{n-1} u(q)^T \cdot B_u(q)^T \cdot \Phi(q+1,n-1)^T\right]\cdot Q \cdot \left[\sum_{r=0}^{n-1}\Phi(r+1,n-1)\cdot B_u(r)\cdot u(r)\right] + \ldots \\ & + \frac{1}{2}\sum_{n=0}^{P-1} u(n)^T \cdot R \cdot u(n) \end{aligned} \quad (14)$$

where,

$$\begin{aligned} S(n) &\equiv Q\cdot\left[\Phi(0,n-1)\cdot x(0)\right] \\ T(n) &\equiv Q\cdot\sum_{m=0}^{n-1}\Phi(m+1,n-1)\cdot B_d(m)\cdot d \end{aligned}$$

Thus, the Hessian and the Jacobian matrices are:

$$\begin{aligned} H_{i,j} &= \sum_{n=\max(i,j)}^{P} B_u(i-1)^T\cdot\Phi(i,n-1)^T\cdot Q\cdot\Phi(j,n-1)\cdot B_u(j-1) + \begin{cases} 0 & i\neq j \\ R & i=j \end{cases} \\ c_j{}^T &= \sum_{n=j}^{P}\left[S^T(n)+T^T(n)\right]\cdot\Phi(j,n-1)\cdot B_u(j-1) \end{aligned} \quad (15)$$

In projectile trajectory optimization, we penalize only the hit point to ensure the target hit. Thus, the optimization problem is reduced to Eq. (16).

$$\begin{aligned} H_{i,j} &= B_u(i-1)^T\cdot\Phi(i,P-1)^T\cdot Q\cdot\Phi(j,P-1)\cdot B_u(j-1) + \begin{cases} 0 & i\neq j \\ R & i=j \end{cases} \\ c_j{}^T &= \left[S^T(P)+T^T(P)\right]\cdot\Phi(j,P-1)\cdot B_u(j-1) \end{aligned} \quad (16)$$

Finally, the de-spun scheme control saturation imposes quadratic constraints on the optimization problem. We choose for the sake of simplicity to specify linear constraints in Eq. (17) instead, and apply an iterative algorithm to find the weight matrix R that will satisfy the quadratic constraints. Other optimization methods, such as a convex optimization, can accommodate quadratic constraints and can be used here as well.

$$A = \begin{bmatrix} [I_P] \\ \hline -[I_P] \end{bmatrix}$$
$$b = \left[\bar{u}(0) \quad \bar{u}(1) \quad \cdots \quad \bar{u}(p-1) \mid \bar{u}(0) \quad \bar{u}(1) \quad \cdots \quad \bar{u}(p-1) \right]^T \tag{17}$$

Together, Eqs. (12), (16) and (17) formulate the quadratic programming problem, to be solved with typical optimization algorithms.

In order to generate the inputs of the optimal trajectory, a reference signal and a discretization sampling rate need to be selected. The reference signal is the desired diversion of the projectile from the uncontrolled trajectory. We select a reference signal that will demonstrate the maximum projectile maneuverability with control signals approaching their saturation levels. Zero Order Hold (ZOH) discretization is applied on the plant, assuming that the linear plant model does not vary by much, as Sandberg assumed in a case study of LTV system model reduction in [20]. The discretization sampling rate of a system controlled by the de-spun scheme does not need to be higher than the nutation frequency. A reference signal of 13.7 m diversion and discretization sampling rate of 30 Hz provide a reasonable trade-off between the size of the optimization problem and control authority. The reference diversion is approximately 90% of the 14.9 m dispersion radius that the open loop de-spun scheme delivers, to provide sufficient control authority saturation margins. The control authority margins were introduced to allow the controller to correct for

system non-linearities and deliver a zero hit point error with the non-linear model. The open loop inputs were applied both on the linear and the non-linear models, as shown in Fig. 14. The linear model produces a zero hit-point error and unsaturated control signals, as planned. The non-linear model, on the other hand, diverges from the optimal trajectory as expected, and will be corrected with closed loop tracking controllers. The orientation plot shows that the nutation is changing along the trajectory, performing precession based maneuvers to produce the required trajectory diversion.

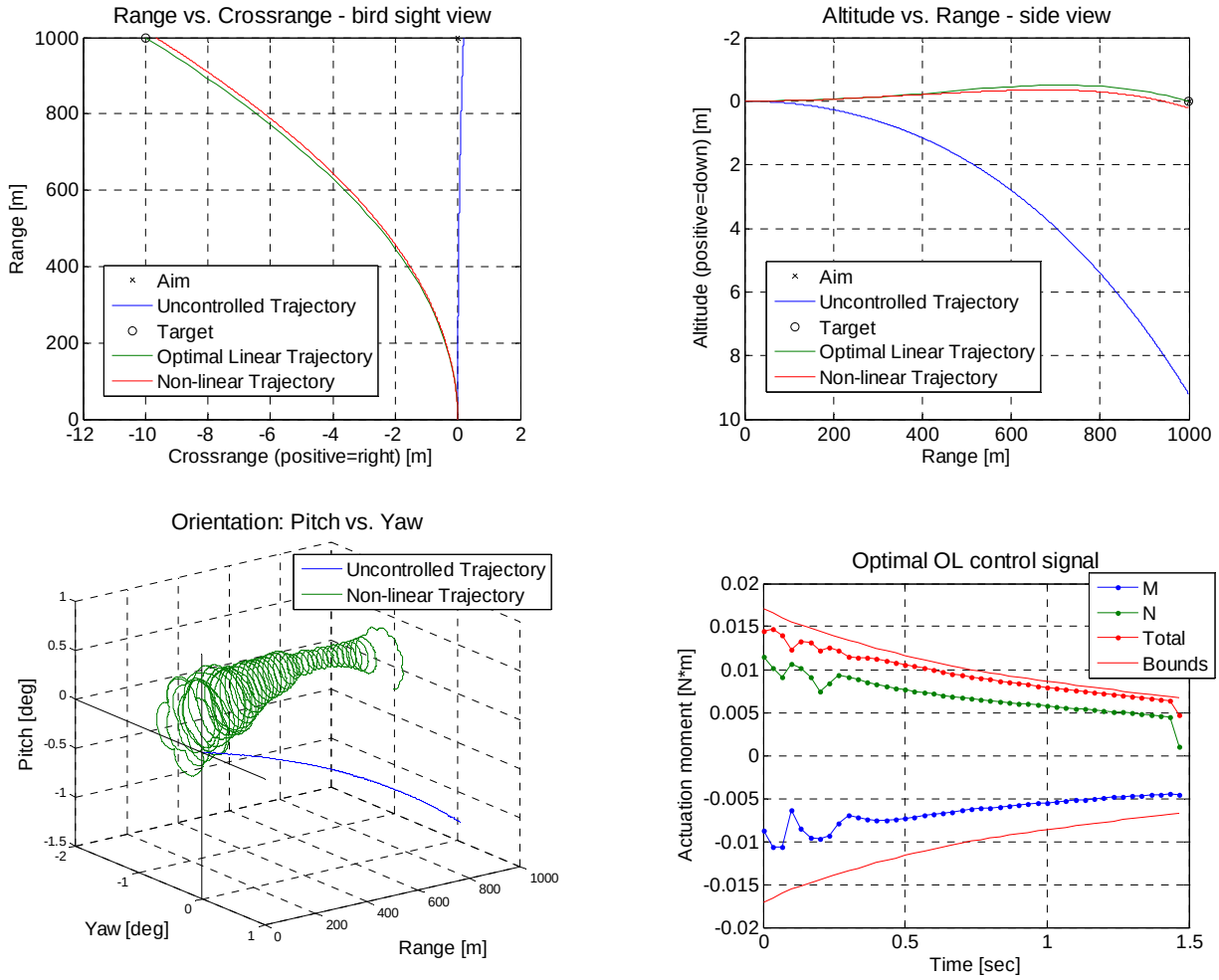

Fig. 14: Optimal Projectile's Trajectory for (y_r,z_r)=(-10,0) reference. Upper left: c.g. bird side view. Upper right: c.g. side view. Bottom left: Projectile orientation (pitch and yaw). Bottom right: Optimal Control signal.

Controllers for Optimal Trajectory Tracking

Next we turn to produce a trajectory tracking controller to follow the optimal trajectory. We assume that the whole state space is available through measurement and estimation. Many tracking controllers exist; we propose to use the minimized quadratic cost LQR and MPC controllers, both are compatible with the quadratic cost objective function in trajectory optimization.

The LQR tracking controller has to account for the LTV plant and changing control saturation levels. We propose gain switching to address both of these requirements. A piecewise set of LQR gain matrices is generated for each time step of the optimal trajectory and the time varying plant and saturation levels are treated as constant within each. The actuator saturation is addressed by partitioning the state space into nested ellipsoids. A non-saturating LQR gain matrix is synthesized for each ellipsoid, by iteratively adjusting the quadratic cost weights, as introduced by Wredenhagen and Belanger in [21]. The gain matrices are computed off-line and stored in the onboard controller memory. Gain switching will occur during flight as the states traverse throughout the state space ellipsoids and time.

The MPC tracking controller re-optimizes the trajectory on-line with real-time measured states and reference signal changes. The on-line optimization problem is a smaller sized variation of the original trajectory optimization. The re-optimization occurs only several times during flight and the prediction horizon recedes as the projectile closes in on the target.

The tracking performance of the proposed controllers is demonstrated in Fig. 15. The controller parameters were selected to demonstrate acceptable performance with the least computation costs: the state space in the LQR controller synthesis was partitioned into 10 ellipsoids per time step and the MPC on-line re-optimization was engaged twice. The superior performance of the MPC tracking controller is demonstrated by the c.g. positions in Fig. 15.a and Fig. 15.b. The precession and nutation images of the two controlled trajectories in Figs. 15.c and Fig. 15.d differ; the MPC creates a similar image to the optimal control (Fig. 14) as expected, while the LQR controlled precision and nutation does not resemble to the optimal trajectory. The wide MPC notation angle near the hit point is indicative of small tracking errors, where the excess control authority is stored in the angular momentum of the projectile. On the other hand, the narrow LQR nutation angle throughout the flight indicates greater tracking errors. Finally, the control signals of the tracking controllers resemble the optimal trajectory with a few exceptions. Both of the controlled signals are discontinuous due to discretization of the plant in trajectory optimization. The LQR control signal shows additional discontinuities due to gain switching. These discontinuities can be eliminated by smoothing the gain transitions. The MPC discontinuities are the inherent result of trajectory re-optimization during flight. Both controllers produce good tracking of the optimal trajectory, where the tradeoffs between performance and computation costs need to be considered.

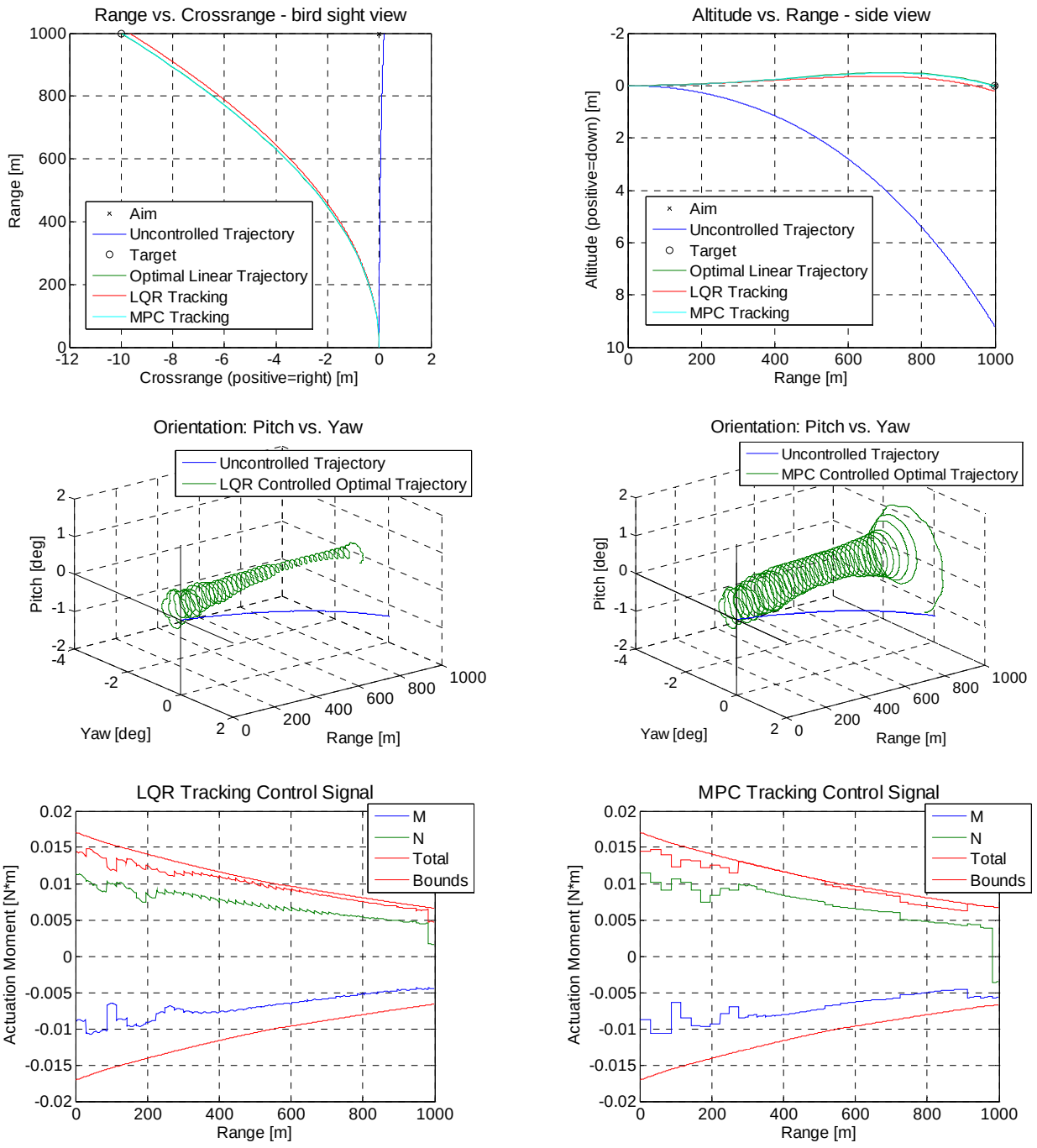

Fig. 15: Optimal trajectory tracking for (y_r,z_r)=(-10,0) reference, using LQR and MPC controllers. (a) upper left: c.g. bird side view. (b) upper right: c.g. side view. (c) middle left: LQR controlled projectile orientation (pitch and yaw). (d) middle right: MPC controlled projectile orientation (pitch and yaw). (e) bottom left: LQR control signal. (f) bottom right: MPC control signal.

CHAPTER 5

DISCUSSION

The different tracking controllers and the trajectory optimization require on-line and off-line computation. Whether the computation is performed on the scope's targeting computer or on a microcontroller onboard the projectile, the computation costs need to be quantified. The trajectory optimization problem can be calculated off-line, before the projectile is launched, for a specific range and a priori known diversion. In our case, the size of the quadratic programming problem that is used to generate the optimal trajectory is dictated by the plant discretization rate, the time of flight and the number of control signals. This turns out to be a $30 \cdot 1.5 \cdot 2 = 90$th rank Hessian matrix and the same number of constraints. The LQR gain matrices are also computed off-line. The number of gain matrices is dictated by the plant discretization rate, the time of flight and the number of state space partitions at each time step. In our case this amounts to $30 \cdot 1.5 \cdot 10 = 450$ gain matrices. Each gain matrix is obtained by solving the Algebraic Ricatti Equation for an eight states plant. The MPC tracking controller on-line computation costs are dictated by the amount of computations performed during flight. Each re-optimization is performed on the remainder of the flight duration. In our example, two equally timed re-optimizations solve 2/3 and 1/3 of the original quadratic programming problem size. Estimation costs are excluded from this discussion but should be included in the system design. The computation costs can be determined once a quadratic programming algorithm is chosen.

A body-fixed flow effector would normally require bandwidths of one to two orders of magnitudes higher than the spin rate, to provide reasonable deployment resolution throughout a roll cycle and sufficient rise time. The high bandwidth actuation required to drive the flow effectors

was reduced with the de-spun scheme to be the spin rate (for a stationary control moment). Tracking an optimal trajectory that was discretized at 30 Hz produces control signals that change at approximately the same rate. The actuation frequency domain would be a frequency modulation of the control signal (modulating frequency) around the spin rate (carrier frequency). Thus, the required actuation bandwidth is the sum of the spin rate and the control signal bandwidth. Jones, Garcia and Waites [22] has shown that this bandwidth scale is feasible with stacked piezo-ceramic actuators.

CHAPTER 6

CONCLUSIONS

The dynamics of a spinning projectile has been studied and utilized to reduce the actuation bandwidth of the trajectory control scheme. The de-spun scheme will produce the largest maneuverability, with a bandwidth requirement as small as the spin rate of the bullet. To utilize the actuation scheme in closed loop trajectory control and accommodate the targeting objective and saturation constraints, a trajectory optimization problem has been formulated. Using linear systems theory, the dynamic model of the projectile was conveniently decoupled, which significantly reduced the computation of the optimization problem. The optimal trajectory was used as a reference for different tracking controllers. The MPC and LQR tracking controllers were evaluated for performance and computation costs. An adequate control authority was demonstrated, keeping the bandwidth and computation requirements feasible with bullets.

CHAPTER 7

FUTURE WORK

The work presented here laid the foundations to several new directions of research in the Laboratory for Intelligent Machine Systems (LIMS) at Cornell University.

In fluid structure interaction, the various flap configurations need to be evaluated for performance and actuation forces. Two parallel efforts are on the way, the first being computational with 3D CFD simulations (Fig. 16) and the second being the experimental validation in a supersonic wind tunnel (Fig. 17, Fig. 18). Currently, both efforts don't take into account the spin of the projectile. While the inclusion of the projectile's spin is believed to be impossible in the experimental effort due to its high rate, it is desirable to combine the dynamics of the projectile with the CFD simulations and account for the spin.

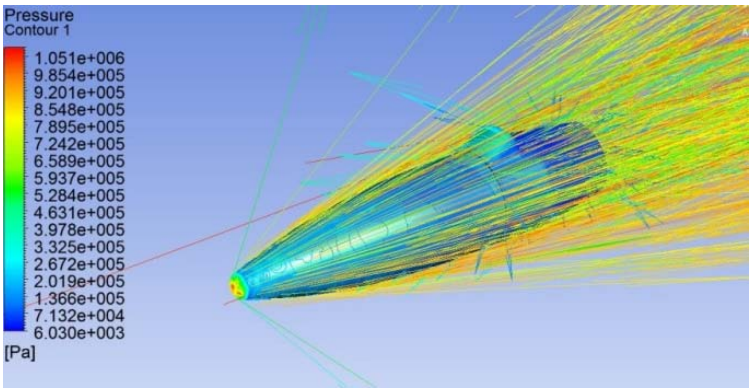

Fig. 16: Preliminary CFD results for the spoiler flow effector.

Fig. 17: CFD results validation setup in the supersonic wind tunnel in Syracuse University.

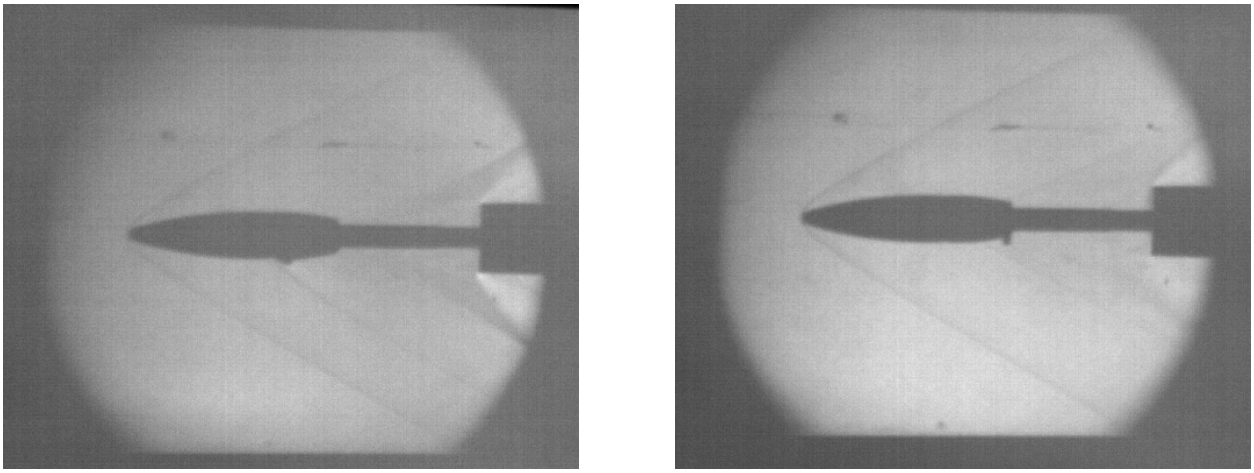

Fig. 18: Schlieren image for the spoiler and gurney flap configurations from the supersonic wind tunnel in Syracuse University.

In actuation, the proposed actuation scheme turn the spotlight to piezoelectric actuators, which excel in transducing high density energy in high frequencies. The small micro-meter scale stroke of these transducers needs to be amplified to achieve the required millimeter scale stroke of the flow effectors. This is possible with stacked transducers (PZT), which can produce tenths of microns. The rest of the mechanical amplification will be obtained with a flexure with two stages: a scissor amplification stage and a lever amplification stage, as shown in Fig. 19. The flexure could be designed to be a part of the projectile shell and body.

The novel actuation scheme proposed in this work requires two bi-directional actuators, oscillating at the frequency of projectile's spin rate. The resonance frequencies of the actuator

assemblies will have to be tuned to be at the desired actuation frequency (the spin rate), to maximize transduction to mechanical energy. We claim that two bi-directional actuators can be enclosed inside a bullet. The preliminary concepts are shown in Fig. 19 and Fig. 20.

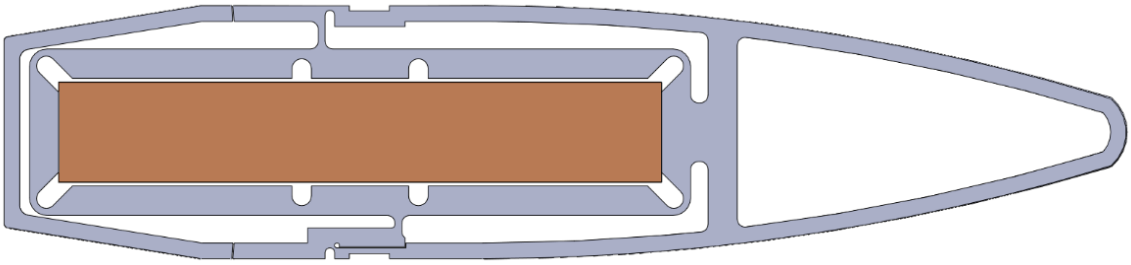

Fig. 19: Mechanical amplification of piezo-electric actuators, for bi-directional spoiler flow effector.

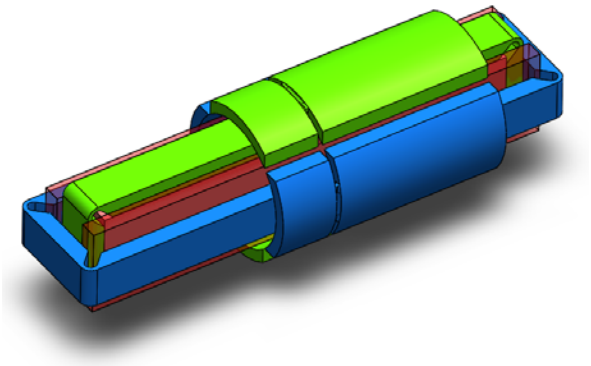

Fig. 20: Packaging two bi-directional actuators in a .50 caliber bullet enclosure.

Finally, in controls, the work presented here may be extended towards a comprehensive system design. For starters, the state estimation challenge is yet to be addressed. The estimator for the projectile state is essential for trajectory control and needs to be tailored with the sensors selection for a given system design. In turn, the model of the projectile should be extended as well, to capture various environmental disturbances, such as wind gusts and atmospheric phenomena, for a better prediction of projectile behavior. Finally, a search for low computation cost optimization algorithms is needed, to allow online optimization on an on-board computer during flight.

APPENDIX

PUBLICATION IN THE JOURNAL OF GUIDANCE CONTROLS AND DYNAMICS

Walking the precession for trajectory control of munitions

Boris Kogan[1] and Ephrahim Garcia[2]
Cornell University, Ithaca, New York, 14853

Introduction

Recent advances in the miniaturization of actuation, sensing and microelectronics have created the opportunities to actively control the flight trajectory of small caliber munitions. Spinning projectiles create challenging constraints and requirements to control systems, including: high bandwidth actuation, relatively short time of flight and the high spin rates [A1]. Limited packing volume for actuators, controllers and energy storage, makes converting a spinning .50 caliber bullet to smart munitions an elusive goal.

Many studies have looked into enabling the trajectory control of spin and fin stabilized munitions. We focus on flight dynamics of projectiles. Fresconi and Polstins [A2], and Ollerenshaw and Costello [A3] looked at the projectile maneuverability and control authority sensitivity. Cooper and Costello [A4] looked into the effects of lateral pulses on a projectile's dynamics. Salman at el. [A5] and Corriveau at el. [A6] investigated the control of a projectile's gyroscopic motion as a means to produce maneuverability. Controlling gyroscopic motion provides an incentive to investigate how it can be utilized to produce control schemes.

---

[1] Graduate Research Assistant, Sibley School of Mechanical and Aerospace Engineering, 138 Upson Hall.
[2] Professor, Sibley School of Mechanical and Aerospace Engineering, 224 Upson Hall, Associate Fellow AIAA.

This analysis explores the dynamics of .50 caliber bullets in a search for features that can be exploited to produce realizable control approaches with achievable actuation requirements. We will discuss how nutation and precession, which are considerably slower than the spin rate, can be controlled in a maneuver we call *walking the precession*. We propose an actuation scheme that generates trajectory control that does not require the munition to be de-spun.

Dynamical Model Analysis

Aerodynamic Model

A review of the forces acting on spin stabilized projectile can be found in McCoy [A7]. The aerodynamic coefficients required for .50 caliber bullets have been determined [A8], providing parameters used in our simulations. Cooper and Costello [A4] provided a nonlinear time varying model for spinning projectiles. This model is used to simulate the projectile trajectory, with a total of 12 states.

Linearized Model and Linear System Analysis

Linearization provides insight into the time variant and non-linear behavior of the spinning projectile. The plane-fixed frame model can be linearized using Taylor Expansion and small angles approximation. The model is linearized assuming small pitch and yaw angles, small transverse linear and angular velocity components, and neglecting products of small quantities with their change rates. As a result, all of the squared AoA terms are nullified, including the nonlinear Magnus effect force. The linear model we use was derived for time derivatives, as opposed to the path derivatives presented by Cooper and Costello [A4].

The forward velocity of the bullet is characterized by Eq. (A1), which shows that the forward velocity is slowed down by the drag force.

$$\dot{\tilde{u}} = -\left(\frac{\pi\rho D^3}{8m} C_{X0}\right) \cdot \frac{1}{D} \cdot \tilde{u}^2 - \frac{1}{m} X_c \tag{A1}$$

The spin rate of the bullet in the linearized model is reduced by the roll damping moment. The spin is coupled to the forward velocity, Eq. (A2).

$$\dot{\tilde{p}} = \left(\frac{\pi \rho D^5 C_{LP}}{16 I_x} \right) \cdot \frac{\tilde{u}}{D} \cdot \tilde{p} \tag{A2}$$

The *transverse velocities* can be formulated by a linear state space in Eq. (A3).

$$\begin{pmatrix} \dot{\tilde{v}} \\ \dot{\tilde{w}} \\ \dot{\tilde{q}} \\ \dot{\tilde{r}} \end{pmatrix} = \left[\hat{A} \right] \cdot \begin{pmatrix} \tilde{v} \\ \tilde{w} \\ \tilde{q} \\ \tilde{r} \end{pmatrix} + \left[\hat{B}_u \right] \cdot \begin{pmatrix} \tilde{M}_c \\ \tilde{N}_c \end{pmatrix} + \left[\hat{B}_d \right] \cdot g \tag{A3}$$

where,

$$\left[\hat{A} \right] = \begin{bmatrix} -\left(\frac{\pi \rho D^3}{8m} C_{NA0} \right) \cdot \frac{\tilde{u}}{D} & 0 & 0 & -\tilde{u} \\ 0 & -\left(\frac{\pi \rho D^3}{8m} C_{NA0} \right) \cdot \frac{\tilde{u}}{D} & \tilde{u} & 0 \\ \left(\frac{\pi \rho D^4 C_{NPA0}}{16 I_y} \right) \cdot \tilde{p} & \left(\frac{\pi \rho D^4 C_{MA0}}{8 I_y} \right) \cdot \frac{\tilde{u}}{D} & \left(\frac{\pi \rho D^5 C_{MQ}}{16 I_y} \right) \cdot \frac{\tilde{u}}{D} & -\left(\frac{I_x}{I_y} \right) \cdot \tilde{p} \\ -\left(\frac{\pi \rho D^4 C_{MA0}}{8 I_y} \right) \cdot \frac{\tilde{u}}{D} & \left(\frac{\pi \rho D^4 C_{NPA0}}{16 I_y} \right) \cdot \tilde{p} & \left(\frac{I_x}{I_y} \right) \cdot \tilde{p} & \left(\frac{\pi \rho D^5 C_{MQ}}{16 I_y} \right) \cdot \frac{\tilde{u}}{D} \end{bmatrix}$$

$$\left[\hat{B}_u \right] = \begin{bmatrix} 0 & 0 \\ 0 & 0 \\ 1/I_y & 0 \\ 0 & 1/I_y \end{bmatrix} \quad \left[\hat{B}_d \right] = \begin{bmatrix} 0 \\ 1 \\ 0 \\ 0 \end{bmatrix}$$

The transverse velocities model of Eq. (A3) has the forward velocity component and the spin rate embedded in the 'A' matrix of the linearized model. The forward velocity and the spin rate equations can be solved separately and then plugged into the linearized transverse model as a time dependent parameters. With that, the transverse velocities model can be treated and analyzed as a Linear Time Variant (LTV) model.

The LTV model comprises two sets of complex poles that vary over the flight of the projectile. The modes can be identified as the gyroscopic precession and nutation of the projectile's motion, i.e., precession frequency range is 16.8-40 Hz and the nutation range is 193.1-206.2 Hz, respectively, over the flight regime. These frequencies are much lower than the spin rate (2.00–2.35 kHz). These dynamics will be utilized for an actuation scheme.

Flow Effectors

We assume flow effectors can be represented as control moments, which manipulate the angular momentum balance. These moments can be generated by devices such as gurney flaps or spoilers [A9], without creating a mass imbalance. These effectors are modeled here as control moments that are generated via asymmetric drag. The lateral aerodynamic forces are not included at this time, since they will not alter the projectile's rigid body dynamics. Once known, the lift forces can be added into the model [A2, A3], and incorporated into a controller synthesis.

The drag force acting on the projectile changes as the velocity greatly varies during flight. We assume the flow effector capacity to be a portion of the overall drag $\Delta C_X/C_X$. This ratio will change as the velocity drops. Since it will only change the maneuverability and not the proposed concepts, we assume it to be constant for the sake of simplicity, and set a maximum at 15% drag asymmetry. The flow effectors' actuators rise time is assumed to be small enough, to avoid lag in deployment.

Open Loop Performance Analysis

Single Actuator Performance

First we will examine the open loop trajectory control of a projectile with a single flow effector. The equations of motion are integrated from a flat-fired initial condition. Our uncontrolled model was validated using the simulations of McCoy [A7]. Next, we set out to define a single actuator open loop control scheme and to compare its performance to the uncontrolled trajectory.

The basic scheme for controlling the trajectory with a single flow effector attached to a spinning body is to deploy the control surface over a prescribed sector of the roll cycle, as illustrated in Fig. A1. We call this control scheme *roll based control* (RBC). As proposed earlier, the model of this flow control concept is a control moment pulse and drag pulse acting through the projectile's center of gravity. The controllable parameters in this scheme are the *moment magnitude* (deployment stroke, pulse height), the *sector size* (deployment time, width of the deployment command pulse) and the *actuation phase* (deployment timing, pulse orientation relative to the gravity vector).

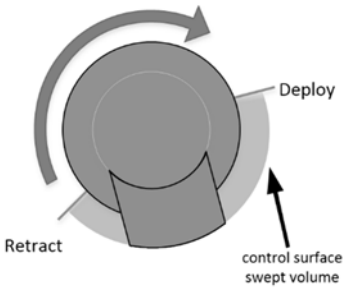

Fig. A1: Roll Based Control scheme, as seen from projectile's rear view.

The RBC produces a noticeable change in the precession and nutation image, as illustrated in Fig. A2 and diverts the projectile from the uncontrolled trajectory, Fig. A3. The control moment pulses change the nutation angle by almost two orders of magnitude resulting in the change of angle of attack, and thus diverting the trajectory. The RBC scheme was investigated by applying the 15% drag asymmetry and the induced moments, via various sector deployments and actuation phases, similar to Fresconi and Plostins [A2]. As shown, different combinations of the control parameters produce a controlled diversion of the hit point.

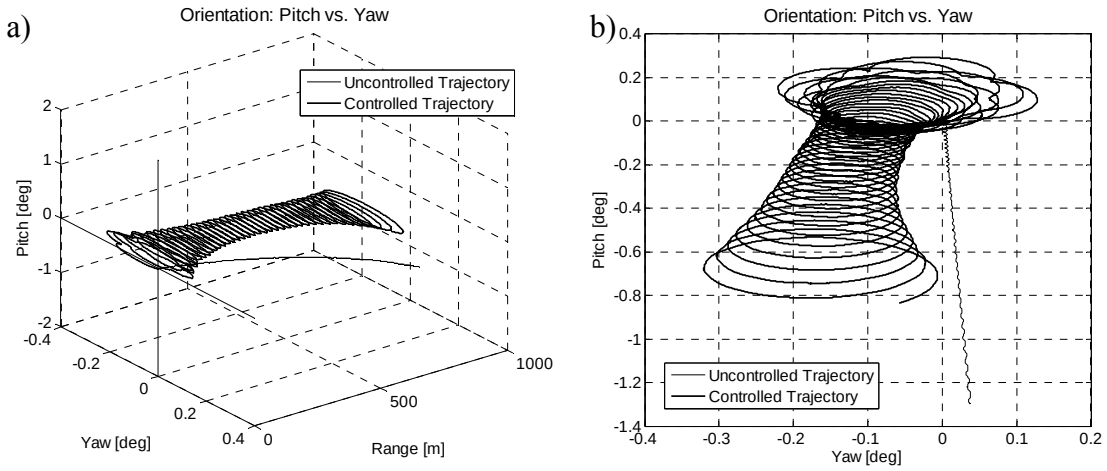

Fig. A2: Uncontrolled and single actuator Roll Controlled trajectories (72° actuation phase, 180° sector size): Projectile orientation (pitch and yaw); (a) 3D view, (b) planar projection.

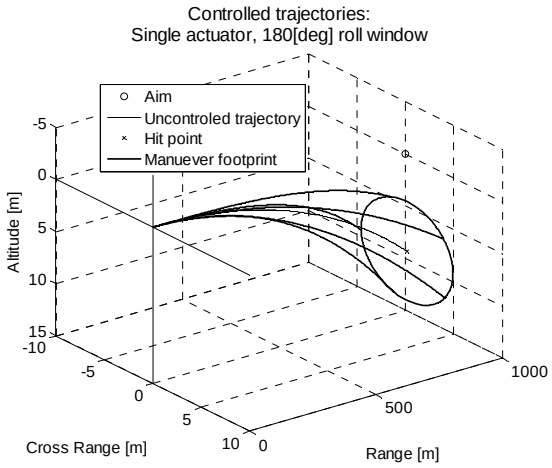

Fig. A3: Uncontrolled trajectory and single actuator maneuverability

Precession Synchronized Single Actuator Performance

A close examination of the RBC trajectory's precession and nutation (Fig. A3) reveals that the scheme has various impacts on angular momentum when the control moments are applied at different precession and nutation states. The projectile is governed by a gyroscopic motion, thus the control moments shift the momentum between angular velocity components, resulting in gyroscopic motion with increased nutation angle. The control moments, when applied at certain precession states, increase the nutation angle, and decrease it when applied at other precession states. This observation implies that the magnitude of the nutation angle can be controlled in an open loop by synchronizing the RBC scheme with the precession rate, and thus controlling only one set of the normal modes of the linearized transverse model. We call this scheme *Precession Synchronized Roll Based Control* (PSRBC). Fig. A4 illustrates the PSRBC scheme, where the precession angle is the transverse component of the angular velocity. To increase the nutation angle, the flow effector deployment is inhibited by masking the actuation command at the precession states where the nutation is reduced, and vise-versa.

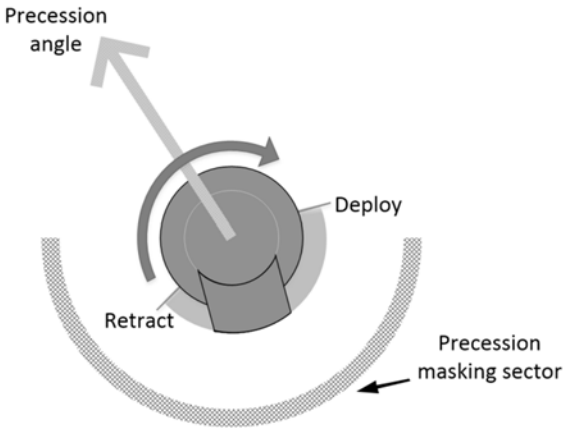

Fig. A4: Precession Synchronized Roll Based Control scheme, as seen from projectile's rear view.

The PSRBC scheme is demonstrated in Fig. A5. Certain combinations of roll and precession masking sectors are able to increase the nutation angle to approximately 1° over 1000 m range, Fig. A5(a), while others minimize the nutation to levels as low as uncontrolled trajectories, Fig. A5(b). This demonstrates that nutation can be controlled and decoupled from precession. Since the transverse linear velocities are coupled to the gyroscopic motion of the projectile, this enables a

controller that could expand and contract the nutation angle to manipulate trajectory [A5, A6]. Repeated expansion and contraction of the nutation at specific states of the precession angle allows us to *walk the precession,* and produce a non-zero average of AoA throughout the precession cycle that changes the bullet trajectory. Close loop trajectory maneuverability can be achieved with active nutation control through trajectory optimization and model predictive controls [A10, A11, A12].

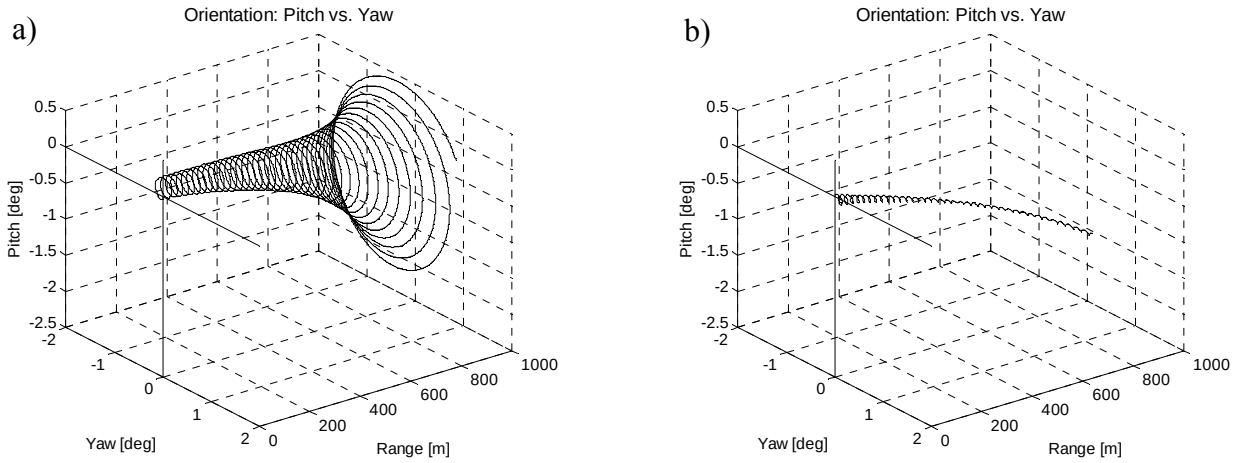

Fig. A5: Uncontrolled and single actuator Precession Synchronized trajectories: Projectile orientation (pitch and yaw). (a): In-phase masking: increasing nutation angle. (b): Out-of-phase masking: decreasing nutation angle.

Two Bi-directional Actuators Performance for the De-spun Effect

Two bi-directional flow effectors, each capable of producing a negative actuation moment by deploying the control surface on the opposite side of the roll sector, can generate an effective control moment that is equivalent to a moment created by a de-spun actuator, even though both actuators are spinning. Thus, the two effectors are capable of creating a moment about the projectile's center of gravity in any direction, regardless of projectile's roll position. This produces an effective *de-spun* scheme with two perpendicular flow effectors, oscillating sinusoidally with 90° phase between them. The scheme produces a continuous and non-rotating moment (stationary with respect to an inertial frame), as illustrated in Fig. A6. The frequency of the flow effectors must be synchronized to the spin rate of the projectile. The orientation of the stationary moment is controlled by introducing a phase shift between the flow effectors oscillation and the gravity vector (roll angle).

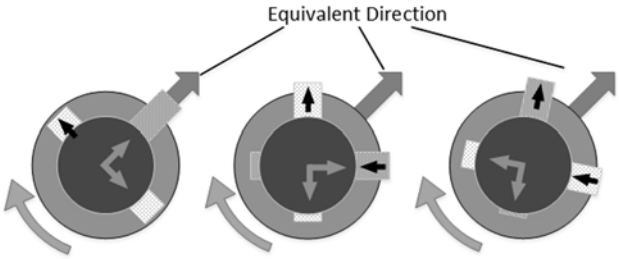

Fig. A6: De-spun flow effectors configuration.

An RBC actuation scheme must be able to deploy a controlled mechanism significantly faster than the deployment time. The later must be a small fraction of the roll cycle. The de-spun scheme has a substantial advantage over any roll based scheme, having a significantly lower actuation bandwidth requirement, being the phase modulation of the desired phase shift bandwidth on the projectile spin rate.

Optimal Open Loop Trajectory

We demonstrate the control capacity of .50 caliber munitions actuated with the de-spun scheme through open loop trajectory optimization. Using insights from the natural frequencies analysis, we attempt to set the re-linearization rate of the LTV model in the optimal trajectory problem formulation to be as low as possible. The maximal possible dispersion radius of the de-spun scheme using 15% drag asymmetry is found to be 14.9 m. A target that would require a 13.7 m diversion from the uncontrolled hit point, and discretization time that corresponds to 30 Hz re-linearization rate are selected, to provide a reasonable trade-off between the size of the optimization problem and control authority. The selected diversion is approximately 90% of the maximal dispersion radius and the de-spun controller remains within the saturation margins. Control authority margins were then introduced to allow the controller to correct for system nonlinearities and to deliver a zero hit point error with closed loop controls. The open loop inputs were applied both on the linear and the non-linear models, as shown in Fig. A7. As expected, the linear model produces a zero hit-point error and the non-linear model diverges from the optimal trajectory, but can be corrected with closed loop controls. The orientation plot shows that the nutation changes along the trajectory, performing precession based maneuvers, to produce the required turns and trajectory diversion. At launch, the optimal trajectory drastically increases the nutation to perform the initial hard turn towards the desired hit point. At mid-range the nutation decreases since there are less trajectory changes made, as the bullet flies towards the target. As the bullet approaches the target, the excess control capacity is transformed into angular momentum, by increasing the nutation. The increased nutation results in a symmetric increase in pitch and yaw and thus the trajectory is not diverted further.

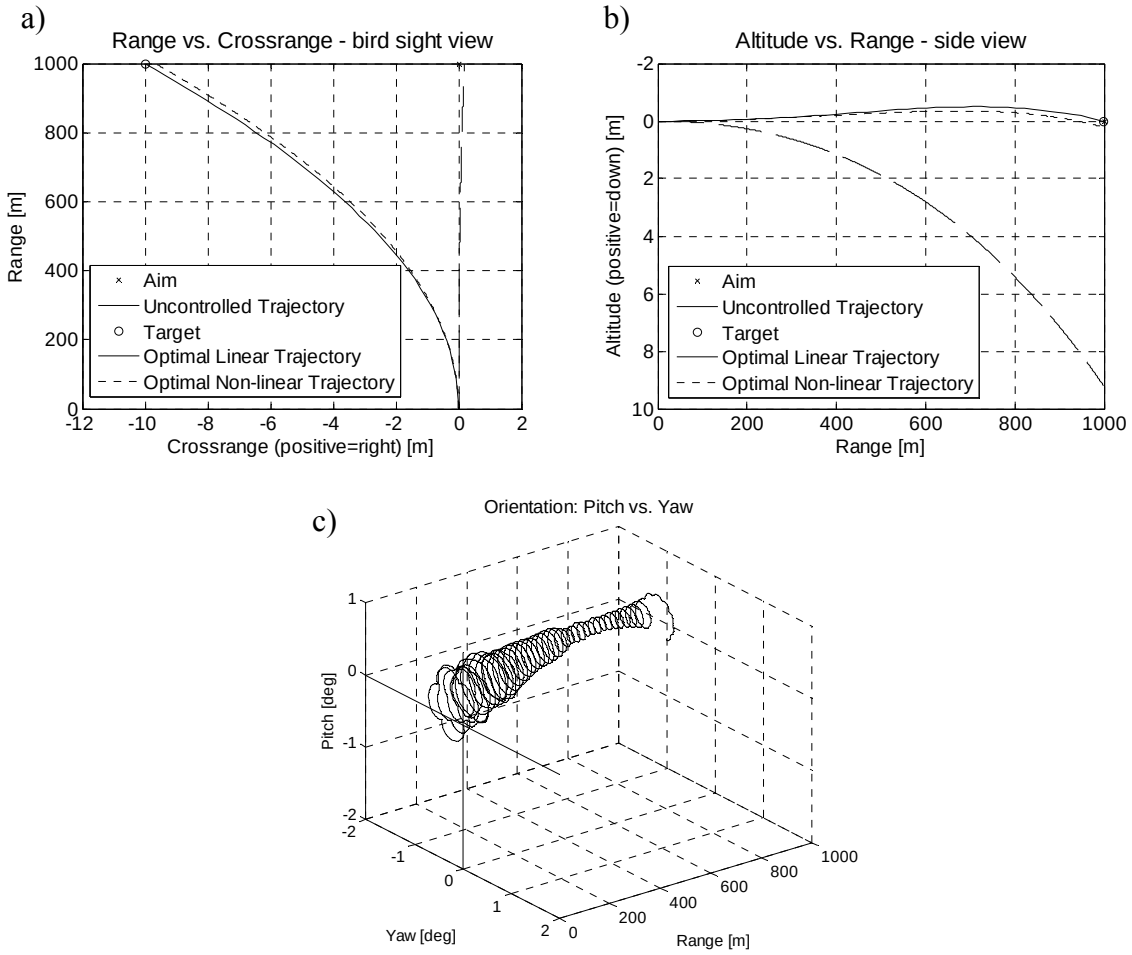

Fig. A7: Optimal Open Loop Trajectory for $(y_r,z_r)=(-10,0)$ reference. (a) bullet's c.g. from bird sight view, (b) bullet's c.g. from side view. (c) Projectile orientation (pitch and yaw).

Conclusions

The challenge of trajectory control of small scale spinning munitions consists of hard controls and actuation bandwidth requirements due to relatively high spin rate, high muzzle velocity and short flight time of projectiles. However, several properties and features of the dynamics of .50 caliber bullets are exploitable in the effort to reduce the actuation bandwidth requirements. This analysis demonstrates that the natural frequencies of the angular velocity transverse components, i.e. the nutation and precession rates, are considerably lower than the spin rate and can be controlled distinctly in a decoupled manner. A novel actuation scheme was shown to produce an effective de-spun control moment with body fixed actuators, requiring significantly lower actuation bandwidth than a standard body fixed actuator. These reduced bandwidth requirements make the actuation of the control mechanisms more feasible.

REFERENCES

[1] McMichael, J., Lovas, A., Plostins, P., Sahu, J.,Brown, G., Glezer, A., “Microadaptive Flow Control Applied to a Spinning Projectile,” Aberdeen Proving Ground, MD: Army Research Laboratory, 2005.

[2] Patil, S., Ng, T., Patel, M, “Trajectory Control of a Small Caliber Projectile Using Active Transpiration,” AIAA Applied Aerodynamics Conference, 25 - 28 June 2007, AIAA 2007-3811, 2007.

[3] Frost, G., and Costello, M., "Control Authority of a Projectile Equipped with an Internal Unbalanced Part," Journal of Dynamic Systems, Measurement, and Control, Vol. 128, No. 4, 2006.

[4] Rogers, J., Costello, M., "Control Authority of a Projectile Equipped with a Controllable Internal Translating Mass," Journal of Guidance, Control, and Dynamics, Vol. 31, No. 5, 2008.

[5] Epperson, E., “Gyroscopically Steerable Bullet,” U.S. Patent 4431150, issued 14 Feb., 1984.

[6] Massey, K., Flick, A., “Mechanical and Jet Actuators for Guiding a Small Caliber Subsonic Projectile,” 25th AIAA Applied Aerodynamics Conference, Miami, FL, 25–28 June 2007, AIAA 2007-3813, 2007.

[7] Lipeles, J., Brosch R. “Guided Bullet,” U.S. Patent 6474593, issued 5 Nov., 2002.

[8] Costello, M., Agarwalla, R., “Improved Dispersion of a Fin Stabilized Projectile Using a Passive Moveable Nose,” Journal of Guidance, Control, and Dynamics, Vol. 23, No. 5, 2000.

[9] Barrett, R., Lee, G., "Design and testing of piezoelectric flight control actuators for hard-launch munitions," Proc. SPIE Conference on Smart Structures and Materials: Smart Structure and Integrated Systems, Vol. 5390, 2004.

[10] Harkins, T., Davis, B., “Drag-Brake Deployment Method and Apparatus for Range Error Correction of Spinning, Gun-Launched Artillery Projectiles,” U.S. Patent 6345785, issued 12 Feb., 2002.

[11] Costello, M., Peterson, A., "Linear Theory of a Dual-Spin Projectile in Atmospheric Flight," Journal of Guidance Control and Dynamics, Vol. 23, No. 5, 2000.

[12] Burchett, B., Peterson, A., Costello, M., “Prediction of Swerving Motion of a Dual-Spin Projectile with Lateral Pulsejets in Atmospheric Flight,” Mathematical and Computer Modeling, Vol. 35, No. 7–8, 2002.

[13] Lipeles, J., “Smart Bullet,” U.S. Patent 6422507, issued 23 Jul., 2002.

[14] Fresconi, F., Cooper, G., Celmins, I., DeSpirito, J., Costello, M., "Flight Mechanics of a Novel Guided Spin-Stabilized Projectile Concept," Proceedings of the Institution of Mechanical Engineers, Part G: Journal of Aerospace Engineering, Vol. 226, No. 3, 2012.

[15] Theodoulis S., Gassmann V., Wernert P., Dritsas L., Kitsios I., Tzes A., "Guidance and control design for a class of spin-stabilized fin-controlled projectiles," Journal of Guidance, Control, and Dynamics, Vol. 36, No. 2, 2013.

[16] McCoy, R., “Modern Exterior Ballistics: The Launch and Flight Dynamics of Symmetric Projectiles,” Atglen, PA: Schiffer Pub, 2012.

[17] McCoy, R., “The Aerodynamic Characteristics of .50 Ball, M33, Api, M8, and Apit, M20 Ammunition,” Ft. Belvoir: Defense Technical Information Center, 1990.

[18] Cooper, G., Costello, M., "Flight Dynamic Response of Spinning Projectiles to Lateral Impulsive Loads," Journal of Dynamic Systems, Measurement, and Control, Vol. 126, No. 3, 2004.

[19] Fresconi, F., Plostins, P., “Control Mechanism Strategies for Spin-Stabilized Projectiles,” Aberdeen Proving Ground, MD: Army Research Laboratory, 2008.

[20] Sandberg, H., "A Case Study in Model Reduction of Linear Time-Varying Systems," Automatica, Vol. 42, No. 3, 2006.

[21] Wredenhagen, G., Bélanger, P., "Piecewise-linear LQ Control for Systems with Input Constraints," Automatica, Vol. 30, No .3, 1994.

[22] Jones, L., Garcia E., Waites, H., "Self-sensing Control as Applied to a PZT Stack Actuator Used as a Micropositioner," Smart Materials and Structures, Vol. 3, No. 2, 1994.

[A1] Barrett, R., Lee, G., "Design and testing of piezoelectric flight control actuators for hard-launch munitions," SPIE 11th Annual International Symposium on Smart Structures and Materials, San Diego, CA, March 2004

[A2] Fresconi, F., Plostins, P., "Control mechanism strategies for spin-stabilized projectiles," Proceedings of the Institution of Mechanical Engineers, Part G: Journal of Aerospace Engineering, Vol. 224, No. 9, 2010.

[A3] Ollerenshaw, D., Costello, M., "Simplified projectile swerve solution for general control inputs," Journal of Guidance, Control, and Dynamics, Vol. 31, No. 5, 2008.

[A4] Cooper, G., Costello, M., "Flight Dynamic Response of Spinning Projectiles to Lateral Impulsive Loads," Journal of Dynamic Systems, Measurement, and Control, Vol. 126, No. 3, 2004.

[A5] Salman, M.U., Chang, B., "Active coning compensation for control of spinning flying vehicles,".Proceedings of the 2010 IEEE International Conference on Control Applications., 2010

[A6] Corriveau D., Wey P., Berner, C., "Thrusters pairing guidelines for trajectory corrections of projectiles," Journal of Guidance, Control, and Dynamics, Vol. 34, No. 4, 2011.

[A7] McCoy, R., "Modern Exterior Ballistics: The Launch and Flight Dynamics of Symmetric Projectiles," Atglen, PA: Schiffer Pub, 2012.

[A8] McCoy, R., **"**The Aerodynamic Characteristics of .50 Ball, M33, Api, M8, and Apit, M20 Ammunition," Ft. Belvoir: Defense Technical Information Center, 1990.

[A9] Dykes, J., Montalvo, C., Costello, M., Sahu, J., "Use of microspoilers for control of finned projectiles," Journal of Spacecraft and Rockets, Vol. 49, No. 6, 2012.

[A10] Burcheff, B., Costello, M., "Model Predictive Lateral Pulse Jet Control of an Atmospheric Rocket," Journal of Guidance, Control, and Dynamics Vol. 25, No. 5, 2002.

[A11] Gross, M., Costello, M., Fresconi, F., “Impact Point Model Predictive Control of a Spin-Stabilized Projectile with Instability Protection,” Proceedings of the Institution of Mechanical Engineers, Part G: Journal of Aerospace Engineering (in-press), 2013.

[A12] Ollerenshaw, D., Costello, M., "Model Predictive Control of a Direct Fire Projectile Equipped With Canards," Journal of Dynamic Systems, Measurement, and Control, Vol. 130m No. 6, 2008.